Estimating winter balance and its uncertainty from direct measurements of snow depth and density on alpine glaciers

Alexandra PULWICKI,[1] Gwenn E. FLOWERS,[1] Valentina RADIĆ,[2]

[1] *Department of Earth Sciences, Faculty of Science, Simon Fraser University, Burnaby, BC, Canada*

[2]*Department of Earth, Ocean and Atmospheric Sciences, Faculty of Science, University of British Columbia, Vancouver, BC, Canada*

Correspondence: Alexandra Pulwicki <apulwick@sfu.ca>

ABSTRACT. Accurately estimating winter surface mass balance on glaciers is central to assessing glacier health and predicting glacier runoff. However, measuring and modelling snow distribution is inherently difficult in mountainous terrain. Here we explore rigorous statistical methods of estimating winter balance and its uncertainty from multiscale measurements of snow depth and density. In May 2016 we collected over 9000 manual measurements of snow depth across three glaciers in the St. Elias Mountains, Yukon, Canada. Linear regression, combined with cross correlation and Bayesian model averaging, as well as ordinary kriging are used to interpolate point-scale values to glacier-wide estimates of winter balance. Elevation and a wind-redistribution parameter exhibit the highest correlations with winter balance, but the relationship varies considerably between glaciers. A Monte Carlo analysis reveals that the interpolation itself introduces more uncertainty than the assignment of snow density or the representation of grid-scale variability. For our study glaciers, the winter balance uncertainty from all assessed sources ranges from 0.03 m w.e. (8%) to 0.15 m w.e. (54%). Despite the challenges associated with estimating winter balance, our results are consistent with a regional-scale winter-balance gradient.

INTRODUCTION

Winter surface mass balance, or "winter balance", is the net accumulation and ablation of snow over the winter season (Cogley and others, 2011), which constitutes glacier mass input. Winter balance (B_w) is half of the seasonally resolved mass balance, initializes summer ablation conditions and must be estimated to simulate energy and mass exchange between the land and atmosphere (e.g. Hock, 2005; Réveillet and others, 2016). Effectively representing the spatial distribution of snow on glaciers is also central to monitoring surface runoff and its downstream effects (e.g. Clark and others, 2011).

Winter balance ~~(WB)~~ is notoriously difficult to estimate (e.g. Dadić and others, 2010; Cogley and others, 2011). Snow distribution in alpine regions is highly variable with short correlation length scales (e.g. Anderton and others, 2004; Egli and others, 2011; Grünewald and others, 2010; Helbig and van Herwijnen, 2017; López-Moreno and others, 2011, 2013; Machguth and others, 2006; Marshall and others, 2006) and is influenced by dynamic interactions between the atmosphere and complex topography, operating on multiple spatial and temporal scales ~~(e.g. Barry, 1992; Liston and Elder, 2006; Clark and others, 2011)~~ (e.g. Barry, 1992; Liston and Elder, 2006; Clark and others, 2011; Scipión and others, 2013). Simultaneously extensive, high resolution and accurate snow distribution measurements on glaciers are therefore difficult to ~~obtain (e.g. Cogley and others, 2011; McGrath and others, 2015). Physically based models are~~ acquire (e.g. Cogley and others, 2011; McGrath and others, 2015) and obtaining such measurements is further complicated by the inaccessibility of many glacierized regions during the winter. Use of physically based models to estimate winter balance is computationally intensive and ~~require~~ requires detailed meteorological data to drive ~~them~~ the models (Dadić and others, 2010). As a result, there is significant uncertainty in estimates of winter balance, thus limiting the ability of models to represent current and projected glacier conditions.

Studies that have focused on obtaining detailed estimates of ~~WB~~ B_w have used a wide range of observational techniques, including direct measurement of snow depth and density (e.g. Cullen and others, 2017), lidar or photogrammerty (e.g. Sold and others, 2013) and ground-penetrating radar (e.g. Machguth and others, 2006; Gusmeroli and others, 2014; McGrath and others, 2015). Spatial coverage of direct measurements is generally limited and often comprises an elevation transect along the glacier centreline (e.g. Kaser and others, 2003). Measurements are ~~often~~ typically interpolated using linear regression on only a few topographic parameters (e.g. MacDougall and Flowers, 2011), with elevation being the most common. Other established techniques include hand contouring (e.g. Tangborn and others, 1975), kriging (e.g. Hock and Jensen, 1999)

and attributing measured winter balance values to elevation bands (e.g. Thibert and others, 2008). Physical snow models have been used to estimate spatial patterns of winter balance (e.g. Mott and others, 2008; Schuler and others, 2008; Dadić and others, 2010) but availability of the required meteorological data generally prohibits their widespread application. Error analysis is rarely undertaken and few studies have thoroughly investigated uncertainty in spatially distributed estimates of winter balance (c.f. Schuler and others, 2008).

More sophisticated snow-survey designs and statistical models of snow distribution are widely used in the field of snow science. Surveys described in the snow science literature are generally spatially extensive and designed to measure snow depth and density throughout a basin, ensuring that all terrain types are sampled. A wide array of measurement interpolation methods are used, including linear (e.g. López-Moreno and others, 2010) and non-linear regressions (e.g. Molotch and others, 2005) that include numerous terrain parameters, as well as geospatial interpolation ~~(e.g. Erxleben and others, 2002)~~ (e.g. Erxleben and others, 2002; Cullen and others, 2017) including various forms of kriging. Different interpolation methods are also combined; for example, regression kriging (see Supplementary Material) adds kriged residuals to a field obtained with linear regression (e.g. Balk and Elder, 2000). Physical snow models such as SnowTran-3D (Liston and Sturm, 1998), Alpine3D (Lehning and others, 2006), and SnowDrift3D (Schneiderbauer and Prokop, 2011) are widely used, and errors in estimating snow distribution have been examined from theoretical (e.g. Trujillo and Lehning, 2015) and applied perspectives (e.g. Turcan and Loijens, 1975; Woo and Marsh, 1978; Deems and Painter, 2006).

The goals of this study are to (1) critically examine methods of converting direct snow depth and density measurements to distributed estimates of winter balance and (2) identify sources of uncertainty, evaluate their magnitude and assess their combined contribution to uncertainty in glacier-wide winter balance. We focus on commonly applied, low-complexity methods of measuring and estimating winter balance in the interest of making our results broadly applicable.

STUDY SITE

The St. Elias Mountains (Fig. 1a) rise sharply from the Pacific Ocean, creating a significant climatic gradient between coastal maritime conditions, generated by Aleutian–Gulf of Alaska low-pressure systems, and interior continental conditions, driven by the Yukon–Mackenzie high-pressure system (Taylor-Barge, 1969). The boundary between the two climatic zones is generally aligned with the divide between the Hubbard and Kaskawulsh Glaciers, approximately 130 km from the coast. Research on snow distribution and glacier mass balance in this area is limited. A series of research programs, including Project "Snow Cornice" and the
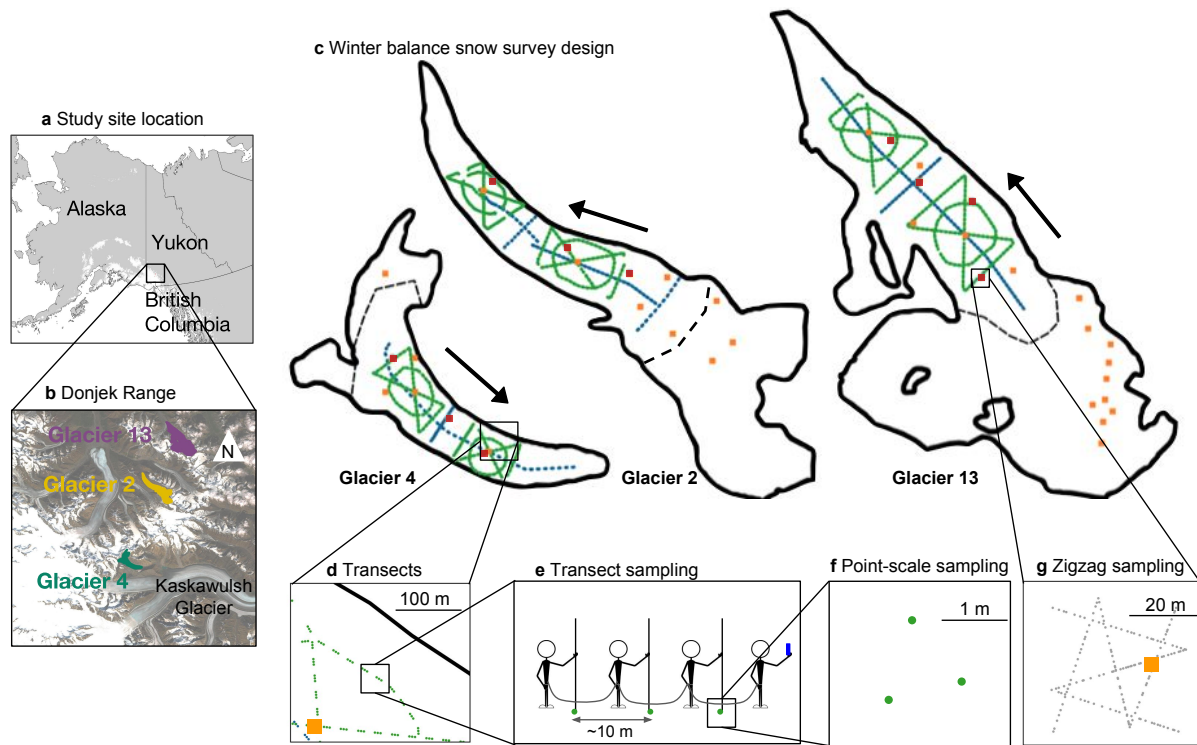
Fig. 1. Study area location and sampling design for Glaciers 4, 2 and 13. (a) Study region in the Donjek Range of the St. Elias Mountains of Yukon, Canada. (b) Study glaciers located along a southwest-northeast transect through the Donjek Range. The local topographic divide is shown as a dashed line. Imagery from Landsat8 (5 September 2013, data available from the U.S. Geological Survey). (c) Details of the snow-survey sampling design, with centreline and transverse transects (blue dots), hourglass and circle designs (green dots) and locations of snow density measurements (orange squares). Arrows indicate ice-flow directions. Approximate location of ELA on each glacier is shown as a black dashed line. (d) Close up of linear and curvilinear transects. (e) Configuration of navigator and observers. (f) Point-scale snow-depth sampling. (g) Linear-random snow-depth measurements in 'zigzag' design (~~grey~~ red dots) with one density measurement (orange square) per zigzag.

86 Icefield Ranges Research Project, were operational in the 1950s and 60s (Wood, 1948; Danby and others,
87 2003) and in the last 30 years, there have been a few long-term studies on selected alpine glaciers (e.g. Clarke,
88 2014) as well as several regional studies of glacier mass balance and dynamics (e.g. Arendt and others, 2008;
89 Burgess and others, 2013; Waechter and others, 2015).
90   We carried out winter balance surveys on three unnamed glaciers in the Donjek Range of the St. Elias
91 Mountains. The Donjek Range is located approximately 40 km to the east of the regional mountain divide
92 and has an area of about $30 \times 30\,\mathrm{km^2}$. Glacier 4, Glacier 2 and Glacier 13 (labelling adopted from Crompton
93 and Flowers (2016)) are located along a southwest-northeast transect through the range (Fig. 1b, Table 1).

Table 1. Physical characteristics of the study glaciers~~and May 2016 winter-balance survey details, including number of snow-depth measurement locations along transects (n_T), total length of transects (d_T), number of combined snow pit and Federal Sampler density measurement locations (n_ρ) and number of zigzag surveys (n_{zz}).~~

	~~Location~~ Location		Elevation (m a.s.l)			Slope (°)	Area
	~~UTM Zone 7~~ UTM Zone 7		*Mean*	*Range*	*ELA*	*Mean*	~~n_T d_T~~ (km²)~~n_ρ n_{zz}~~
height**Glacier 4**	595470 E	6740730 N	2344	1958–2809	∼2500	12.8	3.8 ~~4 7 May 2016 649 13.1 10 3~~
Glacier 2	601160 E	6753785 N	2495	1899–3103	∼2500	13.0	7.0 ~~8 11 May 2016 762 13.6 11 3~~
Glacier 13	604602 E	6763400 N	2428	1923–3067	∼2380	13.4	12.6

These small alpine glaciers are generally oriented southeast-northwest, with Glacier 4 having a predominantly southeast aspect and Glaciers 2 and 13 have generally northwest aspects. The glaciers are situated in valleys with steep walls and have simple geometries. Based on a detailed study of Glacier 2 (Wilson and others, 2013) and related theoretical modelling (Wilson and Flowers, 2013) we suspect all of the study glaciers to be polythermal.

METHODS

Estimating glacier-wide winter balance (B_w) involves transforming measurements of snow depth and density into values of winter balance distributed across a defined grid (b_w). We do this in four steps. (1) Obtain direct measurements of snow depth and density in the field. (2) Assign density values to all depth-measurement

Table 2. Details of the May 2016 winter-balance survey, including number of snow-depth measurement locations along transects (n_T), total length of transects (d_T), number of combined snow pit and Federal Sampler density measurement locations (n_ρ), number of zigzag surveys (n_{zz}), number (as percent of total number of gridcells, and of the number of gridcells in the ablation area) of gridcells sampled (n_S) and the elevation range (as percent of total elevations range and of ablation-area elevation range).

	Date	n_T	d_T (km)	n_ρ	n_{zz}	n_S	Elevation range (m a.s.l.)
Glacier 4	4–7 May 2016	649	13.1	7	3	295 (12%, 21%)	2015–2539 (62%, 97%)
Glacier 2	8–11 May 2016	762	13.6	7	3	353 (8%, 14%)	2151–2541 (32%, 47%)
Glacier 13	12–15 May 2016	941	18.1	~~20~~ 19	4	468 (6%, 14%)	2054–2574 (45%, 62%)

locations to calculate point-scale values of ~~WB~~ b_{w} at each location. (Winter balance, measured in units of metres water equivalent (m w.e.), can be estimated as the product of snow depth and depth-averaged density. (3) Average all point-scale values of b_{w} within each gridcell of a digital elevation model (DEM) to obtain the ~~gricell-averaged WB~~gridcell-averaged b_{w}. (4) Interpolate and extrapolate these gridcell-averaged ~~WB~~ b_{w} values to obtain estimates of ~~WB (in m w.e.) in~~ b_{w} in each gridcell across the domain. B_{w} is then calculated by taking the average of all gridcell-averaged b_{w} values for each glacier. For brevity, we refer to these four steps as (1) field measurements, (2) density assignment, (3) gridcell-averaged ~~WB~~ b_{w} and (4) distributed ~~WB~~ b_{w}. Detailed methodology for each step is outlined below. We use the SPIRIT SPOT-5 DEM (40×40 m) from 2005 (Korona and others, 2009) throughout this study.

Field measurements

Our sampling campaign involved four people and occurred between 5–15 May 2016, which falls within the period of historical peak snow accumulation in southwestern Yukon (Yukon Snow Survey Bulletin and Water Supply Forecast, May 1, 2016). Snow depth is generally accepted to be more variable than density (Elder and others, 1991; Clark and others, 2011; López-Moreno and others, 2013) so we chose a sampling design that resulted in a high ratio (∼55:1) of snow depth to density measurements. In total, we collected more than 9000 snow-depth measurements and more than 100 density measurements throughout the study area (Table **??**tab:GlacierDetails).

During the field campaign there were two small accumulation events. The first, on 6 May 2016, also involved high winds so accumulation could not be determined. The second, on 10 May 2016, resulted in 0.01 m w.e accumulation measured at one location on Glacier 2. Assuming both accumulation events contributed a uniform 0.01 m w.e accumulation to all study glaciers then our survey did not capture ∼3% and ∼2% of estimated B_{w} on Glaciers 4 and 2, respectively. We therefore assume that these accumulation events were negligible and apply no correction. Positive temperatures and clear skies occurred between 11–16 May 2016, which we suspect resulted in melt occurring on Glacier 13. The snow in the lower part of the ablation area of Glacier 13 was isothermal and showed clear signs of melt and metamorphosis. The total amount of melt during the study period was estimated using a degree-day factor for melting snow (Braithwaite, 2008) and found to be small (≤0.01 m w.e., see Supplementary Material) so no corrections were made.

Sampling design

The snow surveys were designed to capture variability in snow depth at regional, basin, gridcell and point scales (Clark and others, 2011). To capture variability at the regional scale we chose three glaciers along

a transect aligned with the dominant precipitation gradient (Fig. 1b) (Taylor-Barge, 1969). To account for basin-scale variability, snow depth was measured along linear and curvilinear transects on each glacier (Fig. 1c) with a sample spacing of 10–60 m (Fig. 1d). Sample spacing was constrained by protocols for safe glacier travel, while survey scope was constrained by the need to complete all surveys within the period of peak accumulation. We selected centreline and transverse transects as the most commonly used survey designs in winter balance studies (e.g. Kaser and others, 2003; Machguth and others, 2006) as well as an hourglass pattern with an inscribed circle, which allows for sampling in multiple directions and easy travel (personal communication from C. Parr, 2016). To capture variability at the grid scale, we densely sampled up to four gridcells on each glacier using a linear-random sampling design (Shea and Jamieson, 2010) we term a 'zigzag'. To capture point-scale variability, each observer made 3–4 depth measurements within ~1 m (Fig. 1ef) at each transect measurement location. ~~In total, we collected more than 9000 snow-depth measurements throughout the study area (Table ??tab:GlacierDetails).~~

Snow depth: transects

~~Winter balance can be estimated as the product of snow depth and depth-averaged density. Snow depth is generally accepted to be more variable than density (Elder and others, 1991; Clark and others, 2011; López-Moreno and others, 2013) so we chose a sampling design that resulted in a high ratio (~55:1) of snow depth to density measurements. Our sampling campaign involved four people and occurred between 5–15 May 2016, which falls within the period of historical peak snow accumulation in southwestern Yukon (Yukon Snow Survey Bulletin and Water Supply Forecast, May 1, 2016).~~ While roped-up for glacier travel with fixed distances between observers, the lead observer used a single-frequency GPS unit (Garmin GPSMAP 64s) to navigate between predefined transect measurement locations (Fig. 1e). The remaining three observers used 3.2 m graduated aluminum avalanche probes to make snow-depth measurements (Kinar and Pomeroy, 2015). The locations of each set of depth measurements, made by the second, third and fourth observers, are estimated using the recorded location of the first observer, the approximate distance between observers and the direction of travel. The 3–4 point-scale depth measurements are averaged to obtain a single depth measurement at each transect measurement location. When considering snow variability at the point scale as a source of uncertainty in snow depth measurements, we find that the mean standard deviation of point-scale snow depth measurements is found to be <7% of the mean snow depth for all study glaciers.

162 Snow-depth sampling was concentrated in the ablation area to ensure that only snow from the current

163 accumulation season was measured. The boundary between snow and firn in the accumulation area can be

164 difficult to detect and often misinterpreted, especially when using an avalanche probe (Grünewald and others,

165 2010; Sold and others, 2013). We intended to use a firn corer to measure winter balance in the accumulation

166 area, but cold snow combined with positive air temperatures led to cores being unrecoverable. Successful

167 snow depth ~~and density~~ measurements within the accumulation area were made either in snow pits or using

168 a Federal Sampler (described below) to unambiguously identify the snow–firn transition.

Snow depth: zigzags

170 ~~To capture snow-depth variability within a single DEM gridcell, we implemented a linear-random zigzag~~

171 ~~sampling design (Shea and Jamieson, 2010).~~ We measured depth at random intervals of 0.3–3.0 m along two

172 'Z'-shaped patterns (Shea and Jamieson, 2010), resulting in 135–191 measurements per zigzag, within three

173 to four ~~40 × 40~~ 40×40 m gridcells (Fig. 1g) per glacier. Random intervals were machine-generated from a

174 uniform distribution in sufficient numbers that each survey was unique. Zigzag locations were randomly

175 chosen within the upper, middle and lower regions of the ablation area of each glacier. ~~A fourth zigzag was~~

176 ~~measured~~ Extra time in the field allowed us to measure a fourth zigzag on Glacier 13 in the central ablation

177 area at ∼2200 m a.s.l.

Snow density

179 Snow density was measured using a Snowmetrics wedge cutter in three snow pits on each glacier~~, as~~

180 ~~well as with a Geo Scientific Ltd. metric Federal Sampler.~~ . Within the snow pits (SP), we measured

181 a vertical density profile (in ~~5~~ 10 cm increments) with the ~~5 × 10 × 10~~ $5 \times 5 \times 10$ cm wedge-shaped

182 cutter (250 cm^3) and a Presola 1000 g spring scale ~~(e.g. Gray and Male, 1981; Fierz and others, 2009)~~

183 (e.g. Gray and Male, 1981; Fierz and others, 2009; Kinar and Pomeroy, 2015). Wedge-cutter error is ap-

184 proximately ±6% (e.g. Proksch and others, 2016; Carroll, 1977). Uncertainty in estimating density from

185 ~~snow-pit~~ SP measurements also stems from incorrect assignment of density to layers that cannot be sampled

186 (e.g. ice lenses and hard layers). We attempt to quantify this uncertainty by varying estimated ice-layer

187 thickness by ±1 cm (≤100%) of the recorded thickness, ice layer density between 700 and 900 kg m^{-3} and

188 the density of layers identified as being too hard to sample (but not ice) between 600 and 700 kg m^{-3}.

189 When considering all three sources of uncertainty, the range of integrated density values is always less than

190 15% of the reference density. Depth-averaged densities for shallow pits (<50 cm) that contain ice lenses are

191 particularly sensitive to changes in prescribed density and ice-lens thickness.

While SP provide the most accurate measure of snow density, digging and sampling a SP is time and labour intensive. Therefore, a Geo Scientific Ltd. metric Federal Sampler (FS) (Clyde, 1932) with a 3.2–3.8 cm diameter sampling tube, which directly measures depth-integrated snow-water equivalent, was used to augment the SP measurements. A minimum of three FS measurements were taken at each of 7–19 locations on each glacier and an additional eight FS measurements were co-located with two SP profiles for each glacier. Measurements for which the snow core length inside the sampling tube was less than 90% of the snow depth were discarded. Densities at each measurement location (eight at each SP, three elsewhere) were then averaged, with the standard deviation taken to represent the uncertainty.

The mean standard deviation of FS-derived density was ≤4% of the mean density for all glaciers.

Density assignment

Measured snow density must be interpolated or extrapolated to estimate point-scale b_w at each snow-depth sampling location. We employ four commonly used methods to interpolate and extrapolate density (Table 3): (1) calculate mean density over an entire mountain range (e.g. Cullen and others, 2017), (2) calculate mean density for each glacier (e.g. Elder and others, 1991; McGrath and others, 2015), (3) linear regression of density on elevation for each glacier (e.g. Elder and others, 1998; Molotch and others, 2005) and (4) calculate mean density using inverse-distance weighting (e.g. Molotch and others, 2005) for each glacier. Densities derived from SP and FS measurements are treated separately, for reasons explained below, resulting in eight possible methods of assigning density.

Gridcell-averaged winter balance

We average one to six (mean of 2.1 measurements) point-scale values of b_w within each DEM gridcell to obtain the gricell-averaged b_w. The locations of individual measurements have uncertainty due to the error in the horizontal position given by the GPS unit and the estimation of observer

Table 3. Eight methods used to estimate snow density at unmeasured locations. Total number of resulting density values given in parentheses, with n_T the total number of snow-depth measurement locations along transects (Table 1).

Method code	Source of measured snow density		Density assignment method
	Snow pit	*Federal Sampler*	
S1	■		Mean of measurements
F1		■	across all glaciers (1)
S2	■		Mean of measurements
F2		■	for each glacier (3)
S3	■		Regression of density on
F3		■	elevation for a glacier (n_T)
S4	■		Inverse distance weighted
F4		■	mean for a glacier (n_T)

location based on the recorded GPS positions of the navigator. This location uncertainty could result in the incorrect assignment of a point-scale ~~WB~~ b_w measurement to a particular gridcell. However, this source of error is not further investigated because we assume that the uncertainty ~~in gridcell-averaged WB~~ resulting from incorrect locations of point-scale b_w values is captured in the ~~zigzag measurements~~ uncertainty derived from zigzag measurements, as described below. ~~Uncertainty~~ Error due to having multiple observers ~~was also evaluated . There are~~ is also evaluated by conducting an analysis of variance (ANOVA) of snow-depth measurement along a transect and testing for differences between observers. We find no significant differences between snow-depth measurements made by observers along any transect (p>0.05), with the exception of the first transect on Glacier 4 (51 measurements)~~.~~, where snow depth values collected by one observer were, on average, greater than the snow depth measurements taken by the other two observers (p<0.01). Since this was the first transect completed and the only one to show differences by observer, this difference can be considered an anomaly. We therefore assume that observer bias does not affect the results of this study and no corrections to the data based on observer are applied.

Distributed winter balance

Gridcell-averaged values of ~~WB~~ b_w are interpolated and extrapolated across each glacier using linear regression (LR) and ~~simple kriging (SK~~ ordinary kriging (OK). The ~~regression~~ LR relates gridcell-averaged

~~WB and b_{w} to~~ various topographic parameters ~~, as this method~~ and we use this method because it is simple and has precedent for success (e.g. McGrath and others, 2015). Instead of a basic ~~regression~~ LR however, we use cross-validation ~~and~~ to prevent data overfitting as well as model averaging to ~~test~~ allow for all combinations of the chosen topographic parameters. We compare the ~~regression approach with simple kriging (SK)~~ LR approach with OK, a data-driven interpolation method free of any physical interpretation (e.g. Hock and Jensen, 1999).

Linear regression

In the ~~regression~~ LR, we use commonly applied topographic parameters as in McGrath and others (2015), including elevation, slope, aspect, curvature, "northness" and a wind-redistribution parameter (Sx from Winstral and others (2002)); we add distance-from-centreline as an additional parameter. Topographic parameters are standardized for use in the LR. For details on data and methods used to estimate the topographic parameters see the Supplementary Material and Pulwicki (2017). Our sampling design ensured that the ranges of topographic parameters associated with our measurement locations represent more than 70% of the total area of each glacier (except elevation on Glacier 2, where our measurements captured only 50%). ~~Topographic parameters are standardized and then weighted by~~

The goal of the LR is to obtain a set of fitted regression coefficients (β_i) ~~calculated by minimizing the sum of squares of the vertical deviations of each datum from the regression line (Davis and Sampson, 1986). For details on data and methods used to estimate the topographic parameters see the Supplementary Material.~~

~~To~~ that correspond to each topographic parameter and to a model intercept. The LR implemented in this study is an extension of a basic multiple linear regression; we use cross-validation to avoid overfitting the data and model averaging to incorporate every possible combination of topographic parameters~~, cross-validation and model averaging are implemented.~~.

First, cross-validation is used to obtain a set of β_i ~~values~~ that have the greatest predictive ability (Kohavi and others, 1995). We randomly select 1000 subsets of the data (2/3 of the values) ~~to fit the LR and~~ and fit a basic multiple linear regression (implemented in MATLAB) to the data subsets, thus obtaining 1000 sets of β_i. The basic multiple linear regression calculates a set of β_i by minimizing the sum of squares of the vertical deviations of each datum from the regression line (Davis and Sampson, 1986). Distributed b_{w} is then calculated using each set of β_i by weighting topographic parameters by their corresponding β_i values for all DEM gridcells. We then use the remaining data (1/3 of the values) to calculate a root mean squared

267 error (RMSE) ~~(Kohavi and others, 1995)~~between the estimated b_w and the observed b_w for corresponding

268 locations. From the 1000 sets of β_i values, we select the set that results in the lowest RMSE.

269 Second, we use model averaging to account for uncertainty when selecting predictors and to maximize the

270 model's predictive ability (Madigan and Raftery, 1994). Models are generated by calculating a set of β_i (as

271 described above) for all possible combinations of topographic parameters~~,~~ resulting in 2^7 models (i.e. 2^7

272 sets of β_i with the greatest predictive ability for each linear combination of topographic parameters). Using

273 a Bayesian framework, model averaging involves weighting all models by their posterior model probabilities

274 (Raftery and others, 1997). ~~To obtain the final regression coefficients, the β_i values from each model are~~

275 ~~weighted according to the~~ We weight the models according to their relative predictive success~~of the model~~,

276 as assessed by the value of the Bayesian Information Criterion (BIC) (Burnham and Anderson, 2004). BIC

277 penalizes more complex models, which further reduces the risk of overfitting. The ~~distributed WB is then~~

278 final set of β_i is then the weighted sum of β_i from all models. Distributed b_w is obtained by applying the

279 ~~resulting regression coefficients~~ final set of β_i to the topographic parameters associated with each gridcell.

~~Simple~~ Ordinary kriging

281 ~~Simple kriging (SK)~~ Kriging is a data-driven method of estimating variables at unsampled locations by

282 using the isotropic spatial correlation (covariance) of measured values to find a set of optimal weights

283 (Davis and Sampson, 1986; Li and Heap, 2008). ~~Simple kriging~~ Kriging assumes spatial correlation between

284 sampling locations that are distributed across a surface and then applies the correlation to interpolate

285 between these locations. Many forms of kriging have been developed to accommodate different data types

286 (e.g. Li and Heap, 2008, and sources within). Ordinary kriging (OK) is the most basic form of kriging where

287 the mean of the estimated field is unknown. Unlike LR, OK is not useful for generating hypotheses to explain

288 the physical controls on snow distribution, nor can it be used to estimate winter balance on unmeasured

289 glaciers. However, we chose to use OK because it does not require external inputs and is therefore an

290 interpretation-free method of obtaining B_w.

291 We used the `DiceKriging` R package (Roustant and others, 2012) to calculate the maximum likelihood

292 covariance matrix, as well as the range distance (θ) and nugget for gridcell-averaged values of winter balance.

293 The range distance is a measure of data correlation length and the nugget is the residual that encompasses

294 sampling-error variance as well as the spatial variance at distances less than the minimum sample spacing

295 (Li and Heap, 2008). ~~Unlike topographic regression, simple kriging is not useful for generating hypotheses~~

296 ~~to explain the physical controls on snow distribution, nor can it be used to estimate winter balance on~~

297 ~~unmeasured glaciers~~A Matére covariance function with $\nu = 5/2$ is used to define a stationary and isotropic

298 covariance and covariance kernels are parameterized as in Rasmussen and Williams (2006).

Uncertainty analysis using a Monte Carlo approach

300 Three sources of uncertainty are considered separately: the uncertainty due to (1) grid-scale variability of

301 b_{w} (σ_{GS}), (2) the assignment of snow density (σ_ρ) and (3) interpolating and extrapolating gridcell-averaged

302 values of b_{w} (σ_{INT}). To quantify the uncertainty of grid-scale and interpolation uncertainty on estimates

303 of ~~glacier-wide WB~~ B_{w} we conduct a Monte Carlo analysis, which uses repeated random sampling of

304 input variables to calculate a distribution of output variables (Metropolis and Ulam, 1949). We repeat

305 the random sampling process 1000 times, resulting in a distribution of values of the ~~glacier-wide WB~~ B_{w}

306 based on uncertainties associated with the four steps outlined above. ~~We use the standard deviation of~~

307 ~~this distribution as a useful metric of uncertainty on the glacier-wide WB. Three~~ Individual sources of

308 uncertainty are ~~considered separately: the uncertainty due to (1) grid-scale variability of WB (σ_{GS}), (2)~~

309 ~~the assignment of snow density (σ_ρ) and (3) interpolating and extrapolating gridcell-averaged values of WB~~

310 ~~(σ_{INT}). These individual sources of uncertainty are~~ propagated through the conversion of snow depth and

311 density measurements to ~~glacier-wide WB~~B_{w}. Finally, the combined effect of all three sources of uncertainty

312 on the ~~glacier-wide WB~~ B_{w} is quantified. We use the standard deviation of the distribution of B_{w} as a useful

313 metric of B_{w} uncertainty. Density assignment uncertainty is calculated as the standard deviation of the eight

314 resulting values of B_{w}. We calculate a relative uncertainty, as the normalized sum of differences between

315 every pair of one hundred distributed ~~WB~~ b_{w} estimates including σ_{GS} and σ_{INT}, to investigate the spatial

316 patterns in b_{w} uncertainty.

Grid-scale uncertainty (σ_{GS})

318 We make use of the zigzag surveys to quantify the true variability of ~~WB~~ b_{w} at the grid scale. Our limited data

319 do not permit a spatially-resolved assessment of grid-scale uncertainty, so we characterize this uncertainty as

320 uniform across each glacier and represent it by a normal distribution. The distribution is centred at zero and

321 has a standard deviation equal to the mean standard deviation of all zigzag measurements for each glacier.

322 For each iteration of the Monte Carlo, ~~WB~~ b_{w} values are randomly chosen from the distribution and added

323 to the values of gridcell-averaged ~~WB~~b_{w}. These perturbed gridcell-averaged values of ~~WB~~ b_{w} are then used

324 in the interpolation. We represent uncertainty in ~~glacier-wide WB~~ B_{w} due to grid-scale uncertainty (σ_{GS}) as

325 the standard deviation of the resulting distribution of ~~glacier-wide WB~~ B_{w} estimates.

Density assignment uncertainty (σ_ρ)

We incorporate uncertainty due to the method of density assignment by carrying forward all eight density interpolation methods (Table 3) when estimating B_{w}. By choosing to retain even the least plausible options, as well as the questionable FS data, this approach results in a generous assessment of uncertainty. We represent the B_{w} uncertainty due to density assignment uncertainty (σ_ρ) as the standard deviation of B_{w} estimates calculated using each density assignment method.

Interpolation uncertainty (σ_{INT})

We represent the uncertainty due to interpolation/extrapolation of gridcell-averaged b_{w} in different ways for LR and OK. LR interpolation uncertainty is represented by a multivariate normal distribution of possible regression coefficients (β_i). The standard deviation of each distribution is calculated using the covariance of β_i as outlined in Bagos and Adam (2015), which ensures that β_i are internally consistent. The β_i distributions are randomly sampled and used to calculate gridcell-estimated b_{w}.

OK interpolation uncertainty is represented by the standard deviation for each gridcell-estimated value of b_{w} generated by the `DiceKriging` package. The standard deviation of B_{w} is then found by taking the square root of the average variance of each gridcell-estimated b_{w}. The final distribution of B_{w} values is centred at the B_{w} estimated with OK. For simplicity, the standard deviation of B_{w} values that result from either LR or OK interpolation/extrapolation uncertainty is referred to as σ_{INT}.

RESULTS

Field measurements

Snow depth

Mean snow depth varied systematically across the study region, with Glacier 4 having the highest mean snow depth and Glacier 13 having the lowest (Fig. 2a). At each measurement location, the median range of measured depths (3–4 points) as a percent of the mean local depth is 2%, 11% and 12%, for Glaciers 4, 2 and 13, respectively. While Glacier 4 has the lowest point-scale variability, as assessed above, it also has the highest proportion of outliers, indicating a more variable snow depth across the glacier. The average
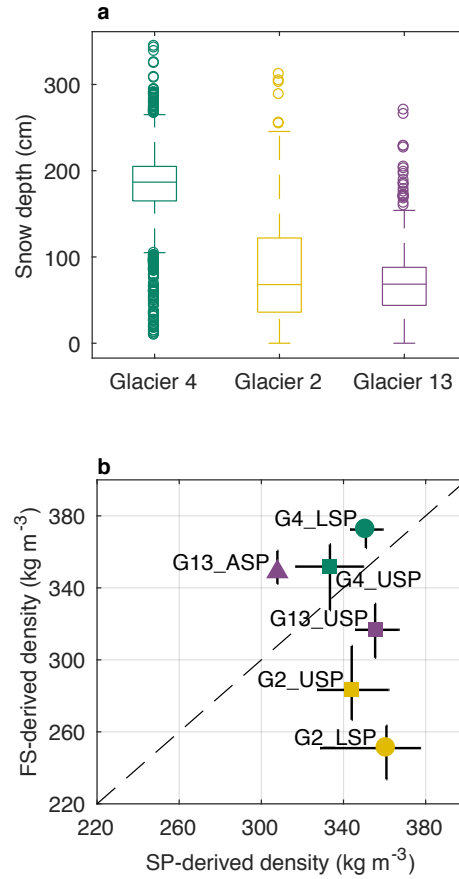
Fig. 2. Measured snow depth and density. (a) Boxplot of measured snow depth on Glaciers 4, 2 and 13 with the first quartiles (box), median (line within box), minimum and maximum values excluding outliers (bar) and outliers (circles), which are defined as being outside of the range of 1.5 times the quartiles (approximately $\pm 2.7\sigma$). (b) Comparison of depth-averaged densities estimated using Federal Sampler (FS) measurements and a wedge cutter in a snow pit (SP) for Glacier 4 (G4), Glacier 2 (G2) and Glacier 13 (G13). Labels indicate ~~snow pit~~ SP locations in the accumulation area (ASP), upper ablation area (USP) and lower ablation area (LSP). Error bars for SP-derived densities are calculated by varying the thickness and density of layers that are too hard to sample, and error bars for FS-derived densities are the standard deviation of measurements taken at one location. One-to-one line is dashed.

standard deviation of all zigzag depth measurements is 0.07 m, 0.17 m and 0.14 m, for Glaciers 4, 2 and 13, respectively. When converted to values of ~~WB~~ b_w using the local FS-derived density measurement, the average standard deviation is 0.027 m w.e., 0.035 m w.e. and 0.040 m w.e. ~~WB~~ Winter-balance data for each zigzag are not normally distributed (Fig. 3).

Snow density

Contrary to expection, co-located FS and SP measurements are found to be uncorrelated ($R^2 = 0.25$, Fig. 2b). The ~~Federal Sampler~~ FS appears to oversample in deep snow and undersample in shallow snow.
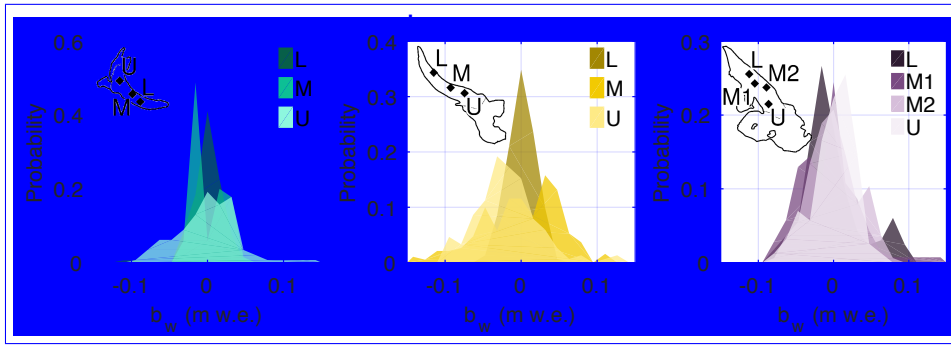
Fig. 3. Distributions of estimated winter-balance values for each zigzag survey in lower (L), middle (M) and upper (U) ablation areas (insets). Local mean has been subtracted. (a) Glacier 4. (b) Glacier 2. (c) Glacier 13.

362 Oversampling by small-diameter ~~(3.2–3.8 cm)~~ sampling tubes has been observed in previous studies, with a
363 percent error between 6.8% and 11.8% (e.g. Work and others, 1965; Fames and others, 1982; Conger and
364 McClung, 2009). Studies that use ~~Federal Samplers~~ FS often apply a 10% correction to all measurements for
365 this reason (e.g. Molotch and others, 2005). Oversampling has been attributed to slots "shaving" snow into
366 the tube as it is rotated (e.g. Dixon and Boon, 2012) and to snow falling into the slots, particularly for snow
367 samples with densities $>400\,\mathrm{kg\,m^{-3}}$ and snow depths $>1\,\mathrm{m}$ (e.g. Beaumont and Work, 1963). Undersampling
368 is likely to occur due to loss of snow from the bottom of the sampler (Turcan and Loijens, 1975). Loss by this
369 mechanism may have occurred in our study, given the isothermal and melt-affected snow conditions observed
370 over the lower reaches of Glaciers 2 and 13. Relatively poor ~~Federal Sampler~~ FS spring-scale sensitivity also
371 calls into question the reliability of measurements for snow depths $<20\,\mathrm{cm}$.

372 Our FS-derived density values are positively correlated with snow depth ($\mathrm{R}^2 = 0.59$). This relationship
373 could be a result of physical processes, such as compaction in deep snow and preferential formation of depth
374 hoar in shallow snow, but is more likely a result of measurement artefacts for a number of reasons. First, the
375 total range of densities measured by the ~~Federal Sampler~~ FS seems improbably large (227–$431\,\mathrm{kg\,m^{-3}}$)~~given~~
376 ~~the conditions at the~~. At the time of sampling the snow pack had little fresh snow, which confounds the
377 low density values, and was not yet saturated and had few ice lenses, which confounds the high density
378 values. Moreover, the range of FS-derived values is much larger than ~~than~~ that of SP-derived values when
379 co-located measurements are compared. Second, compaction effects of the magnitude required to explain the
380 density differences between SP and FS measurements would not be expected at the measured snow depths
381 (up to $340\,\mathrm{cm}$). Third, no linear relationship exists between depth and SP-derived density ($\mathrm{R}^2 = 0.05$). These
382 findings suggest that the ~~Federal Sampler~~ FS measurements have a bias for which we have not identified a

383 suitable correction. Despite this bias, we use FS-derived densities to generate a range of possible b_w estimates

384 and to provide a generous estimate of uncertainty arising from density assignment.

Density assignment

386 Given the lack of correlation between co-located SP- and FS-derived densities (Fig. 2), we use the densities

387 derived from these two methods separately (Table 3). SP-derived regional (S1) and glacier-mean (S2) densities

388 are within one standard deviation of the corresponding FS-derived densities (F1 and F2) although SP-derived

389 density values are larger (see Supplementary Material, Table ~~S2~~S3). For both SP- and FS-derived densities,

390 the mean density for any given glacier (S2 or F2) is within one standard deviation of the mean across all

391 glaciers (S1 or F1). Correlations between elevation and SP- and FS-derived densities are generally high

392 ($R^2 > 0.5$) but vary between glaciers (Supplementary material, Table ~~S2~~S3). For any given glacier, the

393 standard deviation of the 3–4 SP- or FS-derived densities is <13% of the mean of those values (S2 or F2)

394 (Supplementary material, Table ~~S2~~S3). We adopt S2 (glacier-wide mean of SP-derived densities) as the

395 reference method of density assignment. Though the method described by S2 does not account for known

396 basin-scale spatial variability in snow density (e.g. Wetlaufer and others, 2016), it is commonly used in winter

397 balance studies (e.g. Elder and others, 1991; McGrath and others, 2015; Cullen and others, 2017).

Gridcell-averaged winter balance

399 The distributions of gridcell-averaged ~~WB~~ b_w values for the individual glaciers are similar to those in Fig. 2a

400 but with fewer outliers ~~.~~ (see Supplementary Material, Fig. S4). The standard deviations of ~~WB~~ b_w values

401 determined from the zigzag surveys are almost twice as large as the mean standard deviation of point-scale

402 ~~WB~~ b_w values within a gridcell measured along transects ~~.~~ (see Supplementary Material, Fig. S5). However,

403 a small number of gridcells sampled in transect surveys have standard deviations in ~~WB~~ b_w that exceed

404 0.25 m w.e. (∼10 times greater than those for zigzag surveys). ~~We nevertheless assume that the gridcell~~

405 ~~uncertainty is captured with dense sampling in zigzag gridcells.~~

406 ~~Distribution of coefficients (β_i) determined by linear regression of gridcell-averaged WB on DEM-derived~~

407 ~~topographic parameters for the eight different density assignment methods (Table 3). Coefficients are~~

408 ~~calculated using standardized data, so values can be compared across parameters. Regression coefficients~~

409 ~~that are not significant are assigned a value of zero. Topographic parameters include elevation (z), distance~~

410 ~~from centreline (d_C), slope (m), curvature (κ) and wind redistribution (Sx). Aspect (α) and "northness"~~

411 ~~(N) are not shown because coefficient values are zero in every case. The box plot shows first quartiles~~

412 ~~(box), median (line within box), mean (circle within box), minimum and maximum values excluding outliers~~
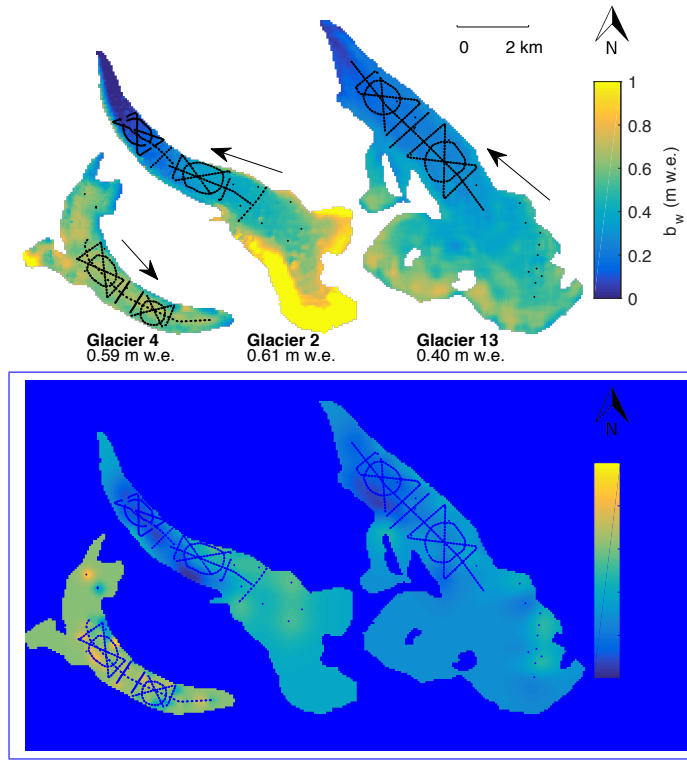
Fig. 4. Spatial distribution of winter balance (~~WB~~b_w) estimated using linear regression (top row) and ~~simple~~ ordinary kriging (bottom row) with densities assigned as per S2 (Table 3). The linear regression method involves multiplying regression coefficients, found using cross validation and model averaging, by topographic parameters for each gridcell. Ordinary kriging uses the covariance of measured values to find a set of optimal weights for estimating values at unmeasured locations. Locations of snow-depth measurements taken in May 2016 are shown as black dots. Ice-flow directions are indicated by arrows. Values of ~~glacier-wide WB~~ B_w are given below labels.

413 ~~(bars) and outliers (gray dots), which are defined as being outside of the range of 1.5 times the quartiles~~

414 ~~(approximately ±2.7σ).~~

Distributed winter balance

416 ~~**Distributed winter balance**~~

417 ~~Relative uncertainty in distributed winter balance (WB) (Fig. ??) found using linear regression (top row)~~

418 ~~and simple kriging (bottom row). Values closer to one indicate higher relative uncertainty. Ice-flow directions~~

419 ~~are indicated by arrows.~~

Linear regression

421 The highest values of estimated b_w are found in the upper portions of the accumulation areas of Glaciers

422 2 and 13 (Fig. 4). These areas also correspond to large values of elevation, slope, and wind redistribution.
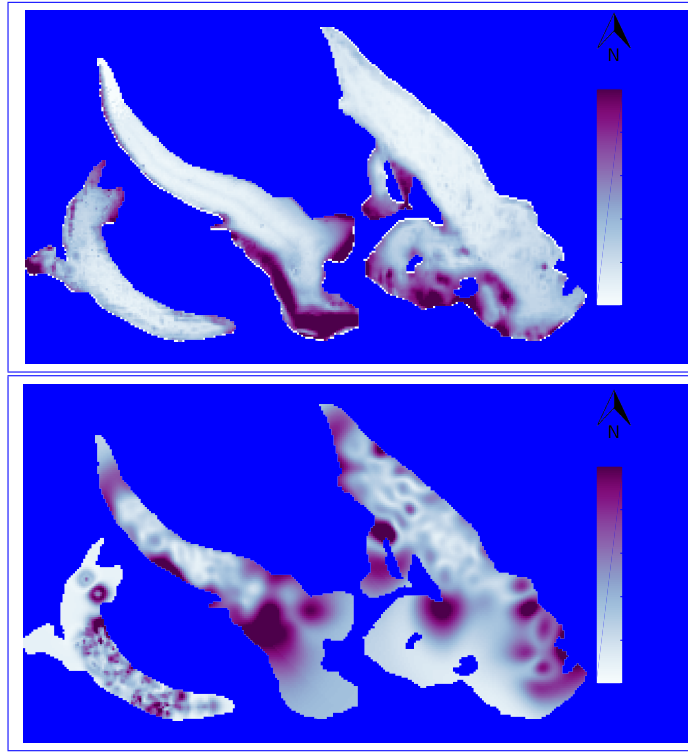
Fig. 5. Relative uncertainty in distributed winter balance (b_{w}) (Fig. 4) found using linear regression (top row) and ordinary kriging (bottom row). Values closer to one indicate higher relative uncertainty. Ice-flow directions are indicated by arrows.

Extrapolation of the positive relation between b_{w} and elevation, as well as slope and Sx for Glacier 2, results in high b_{w} estimates and large relative uncertainty in these estimates (Fig. 5). On Glacier 4, the distributed b_{w} and the relative uncertainty are almost uniform (Fig. 4) due to the small regression coefficients for all topographic parameters. The explained variance of the LR-estimated b_{w} differs considerably between

Table 4. Glacier-wide winter balance (~~WB~~B_{w}, m w.e.) estimated using linear regression and ~~simple~~ ordinary kriging for the three study glaciers. Root mean squared error (RMSE, m w.e.) is computed as the average of all RMSE values between gridcell-averaged values of ~~WB~~ b_{w} (the data) that were randomly selected and excluded from interpolation (1/3 of all data) and those estimated by interpolation. RMSE as a percent of the ~~glacier-wide WB~~ B_{w} is shown in brackets.

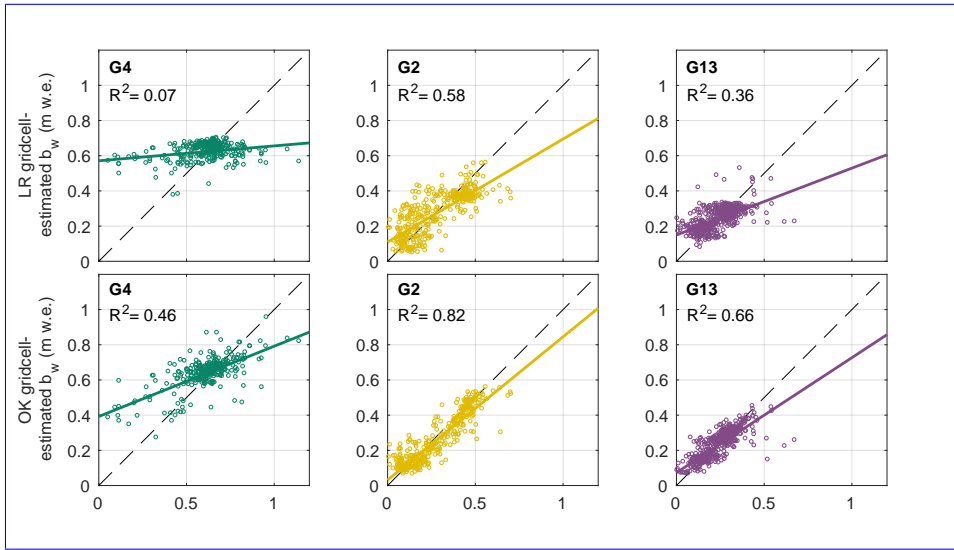|	Linear regression		Ordinary kriging	
	~~WB~~ B_{w}	RMSE	~~WB~~ B_{w}	RMSE
G4	0.58	0.15 (26%)	0.62	~~0.13 (21~~0.11 (18%)
G2	0.58	0.10 (17%)	~~0.37~~ 0.35	~~0.07 (19~~0.06 (18%)
G13	0.38	0.08 (21%)	0.27	~~0.07 (26~~0.06 (21%)

Fig. 6. Winter balance (b_w) estimated by linear regression (LR, top row) or ordinary kriging (OK, bottom row) versus the grid-cell averaged b_w data for Glacier 4 (left), Glacier 2 (middle) and Glacier 13 (right). Each circle represents a single gridcell. Explained variance (R^2) is provided. Best-fit (solid) and one-to-one (dashed) lines are shown.

glaciers (Fig. 6), with the best correlation between modelled- and observed-b_w occurring for Glacier 2. LR is an especially poor predictor of b_w on Glacier 4, where B_w can be estimated equally well using the mean of the data. RMSE is also highest for Glacier 4 (Table 4).

Ordinary kriging

For all three glaciers, large areas that correspond to locations far from measurements have b_w estimates equal to the kriging mean. Distributed b_w estimated with OK on Glacier 4 is mostly uniform except for local deviations close to measurement locations (Fig. 4) and relative uncertainty is highest close to measurement locations. Distributed b_w varies more smoothly on Glaciers 2 and 13 (Fig. 4). Glacier 2 has a distinct region of low estimated b_w (~ 0.1 m w.e.) in the lower part of the ablation area, which corresponds to a wind-scoured region of the glacier. Glacier 13 has the lowest estimated mean b_w and only small deviations from this mean at measurement locations (Fig. 4). Relative uncertainty vary considerably across the three study glaciers with the greatest uncertainty just outside of the region with observed b_w (Fig. 5). As expected, explained variance of OK-estimated b_w is high for both Glaciers 2 and 13 (Fig. 6) because OK is a data-fitting algorithm. However, explained variance (Fig. 6) for Glacier 4 is relatively low and RMSE is relatively high (Table 4), indicating a highly variable distribution of b_w.
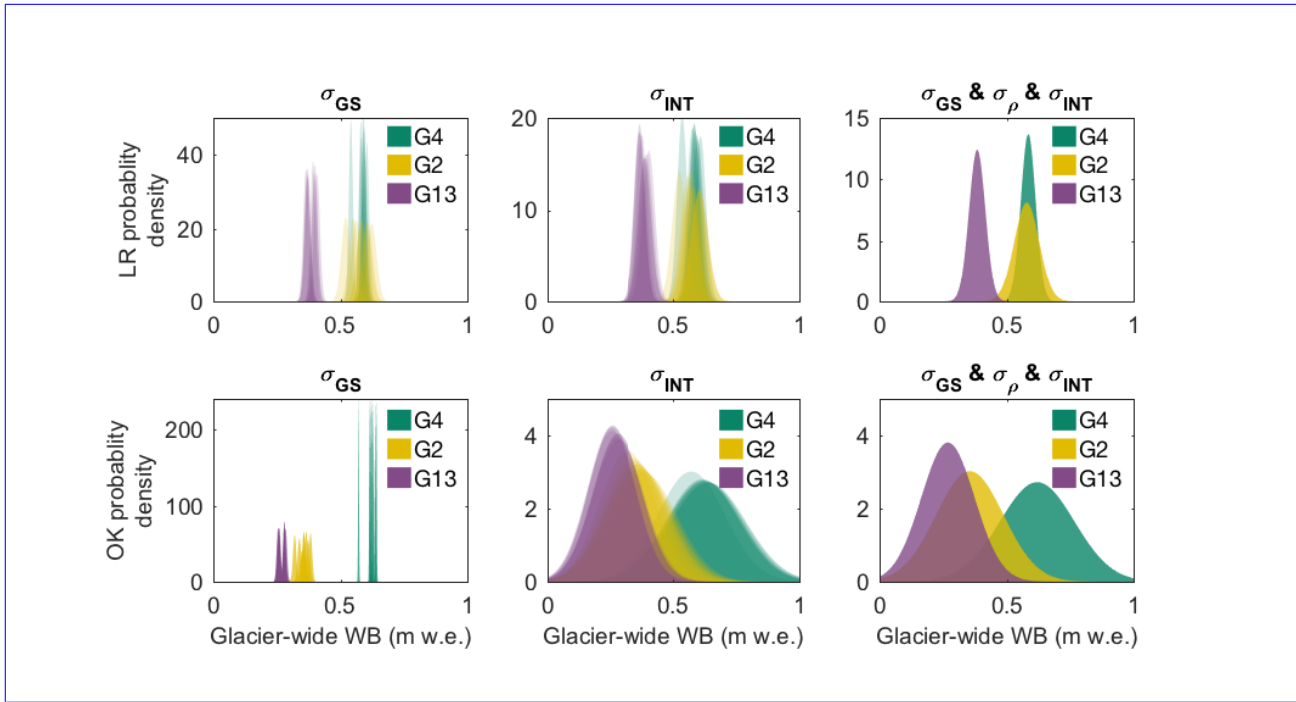
Fig. 7. ~~Winter~~ Distributions of glacier-wide winter balance (~~WB~~B_w) ~~estimated by linear regression~~ for Glaciers 4 (~~LR~~G4), ~~top row~~2 (G2) ~~or simple kriging~~ and 13 (~~SK, bottom row~~G13) ~~versus the grid-cell averaged WB data for Glacier 4~~ that arise from various sources of uncertainty. B_w distribution arising from grid-scale uncertainty (σ_GS) (left column)~~, Glacier 2~~. B_w distribution arising from interpolation uncertainty (σ_{INT}) (middle column). B_w distribution arising from a combination of σ_GS, σ_{INT} and ~~Glacier 13~~ density assignment uncertainty (σ_ρ) (right column). ~~Each circle represents a single gridcell~~Results are shown for interpolation by linear regression (LR, top row) and ordinary kriging (OK, bottom row). ~~Best-fit~~Left two columns include eight distributions per glacier (~~solid~~colour) and ~~one-to-one~~ each corresponds to a density assignment method (~~dashed~~S1–S4 and F1–F4)~~lines are shown~~.

Uncertainty analysis using a Monte Carlo approach

~~Linear Regression~~

Table 5. Standard deviation ($\times 10^{-2}\,\text{m w.e.}$) of glacier-wide winter balance (B_w) distributions arising from uncertainties in grid-scale b_w (σ_GS), density assignment (σ_ρ), interpolation (σ_INT) and all three sources combined (σ_ALL) for linear regression (left columns) and ordinary kriging (right columns)

	Linear regression				Ordinary kriging			
	σ_GS	σ_ρ	σ_{INT}	σ_ALL	σ_GS	σ_ρ	σ_{INT}	σ_ALL
Glacier 4	0.86	1.90	2.13	2.90	0.17	2.16	14.35	14.62
Glacier 2	1.80	3.37	3.09	4.90	0.69	2.01	12.38	13.19
Glacier 13	1.12	1.68	2.80	3.20	0.56	1.29	9.75	10.48

Glacier-wide winter balance is affected by uncertainty introduced by the representativeness of gridcell-averaged values of b_w (σ_{GS}), choosing a method of density assignment (σ_ρ), and interpolating/extrapolating b_w values across the domain (σ_{INT}). Using a Monte Carlo analysis, we find that interpolation uncertainty contributes more to B_w uncertainty than grid-scale uncertainty or density assignment method. In other words, the distribution of B_w that arises from grid-scale uncertainty and the differences in distributions between methods of density assignment are smaller than the distribution that arises from interpolation uncertainty (Fig. 7 and Table 5). The B_w distributions obtained using LR and OK overlap for a given glacier, but the distribution modes differ (Fig. 7). OK-estimated values of b_w in the accumulation area are generally lower (Fig. 4), which lowers the B_w estimate. The uncertainty in OK-estimated values of B_w is large, and unrealistic B_w values of 0 m w.e. can be estimated (Fig. 7).

The values of B_w for our study glaciers (using LR and S2 density assignment method), with an uncertainty equal to one standard deviation of the distribution found with Monte Carlo analysis, are: 0.59 ± 0.03 m w.e. for Glacier 4, 0.61 ± 0.05 m w.e. for Glacier 2 and 0.40 ± 0.03 m w.e. for Glacier 13. The B_w uncertainty from the three investigated sources of uncertainty ranges from 0.03 m w.e (5%) to 0.05 m w.e (8%) for LR estimates and from 0.10 m w.e (37%) to 0.15 m w.e (24%) for ordinary-kriging estimates (Table 4).

DISCUSSION

Distributed winter balance

Linear regression

Of the topographic parameters in the ~~linear regression~~LR, elevation (z) is the most significant predictor of gridcell-averaged ~~WB~~ b_w for Glaciers 2 and 13, while wind redistribution (Sx) is the most significant predictor for Glacier 4 (Fig. 8~~, Fig. ??~~). As expected, gridcell-averaged ~~WB~~ b_w is positively correlated with elevation where the correlation is significant. It is possible that the elevation correlation was accentuated due to melt onset for Glacier 13 in particular. ~~Many studies~~ Glacier 2 had little snow at the terminus likely due to steep ice and wind-scouring but the snow did not appear to have been affected by melt. Our results are consistent with many studies that have found elevation to be the most significant predictor of ~~winter-balance data (e.g. Machguth and others, 2006; McGrath and others, 2015). However, WB elevation gradients vary considerably between glaciers (e.g. Winther and others, 1998) and other factors, such as glacier shape and orientation relative to dominant wind direction, are strong predictors of the winter-balance distribution (Machguth and others, 2006; Grabiec and others, 2011). Some studies find no significant~~
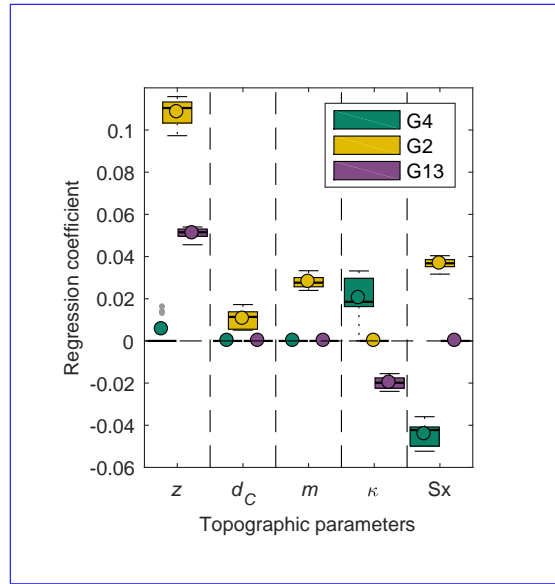
Fig. 8. Distribution of coefficients (β_i) determined by linear regression of gridcell-averaged b_w on DEM-derived topographic parameters for the eight different density assignment methods (Table 3). Coefficients are calculated using standardized data, so values can be compared across parameters. Regression coefficients that are not significant are assigned a value of zero. Topographic parameters include elevation (z), distance from centreline (d_C), slope (m), curvature (κ) and wind redistribution (Sx). Aspect (α) and "northness" (N) are not shown because coefficient values are zero in every case. The box plot shows first quartiles (box), median (line within box), mean (circle within box), minimum and maximum values excluding outliers (bars) and outliers (gray dots), which are defined as being outside of the range of 1.5 times the quartiles (approximately $\pm 2.7\sigma$).

correlation between WB on glaciers and topographic parameters, with seasonal snow accumulation data (e.g. Machguth and others, 2006; Grünewald and others, 2014; McGrath and others, 2015). The b_w–elevation gradient is $13\,\mathrm{mm}/100\,\mathrm{m}$ on Glacier 2 and $7\,\mathrm{mm}/100\,\mathrm{m}$ on Glacier 13. These gradients are consistent with those reported for a few glaciers in Svalbard (Winther and others, 1998) but are considerably smaller than many reported b_w–elevation gradients, which range between 60–240 mm/100 m (e.g. Hagen and Liestøl, 1990; Tveit and Killingtveit, 1994; Winther and others, 1998). Extrapolating linear relationships to unmeasured locations typically results in considerable estimation error, as seen by the large b_w values (Fig. 4) and large relative uncertainty (Fig. 5) in the high-elevation regions of Glaciers 2 and 13. The low correlation between b_w and elevation on Glacier 4 is consistent with Grabiec and others (2011) and López-Moreno and others (2011), who conclude that highly variable distributions of snow can be attributed to complex interactions between topography and the atmosphere that could not cannot be easily quantified (e.g. Grabiec and others, 2011; López-Moreno and others, 2011). Extrapolating relationships to

485 ~~unmeasured locations, especially the accumulation area, is susceptible to large uncertainties (Fig. 5). This~~

486 ~~extrapolation has a considerable effect on values of glacier-wide WB, as the highest values of WB are~~

487 ~~typically found in the accumulation area (Fig. ??).~~ The snow on Glacier 4 also did not appear to have

488 been affected by melt and it is hypothesized that significant wind-redistribution processes, that were not

489 captured by the Sx parameter, covered ice-topography and produced a relatively uniform snow depth across

490 the glacier.

491 Gridcell-averaged ~~WB~~ b_w is negatively correlated with Sx on Glacier 4, counter-intuitively indicating

492 less snow in what would be interpreted as sheltered areas. Gridcell-averaged ~~WB~~ b_w is positively

493 correlated with Sx on Glaciers 2 and 13. ~~Similarly, gridcell-averaged WB is positively correlated with~~

494 ~~curvature on Glacier 4 and negatively correlated on Glaciers 2 and 13. Wind redistribution and~~

495 ~~preferential deposition of snow are known to have a large influence on snow distribution at sub-basin~~

496 ~~scales (e.g. Dadić and others, 2010; Winstral and others, 2013; Gerber and others, 2017). Our~~ Our results

497 corroborate those of McGrath and others (2015) in a study of six glaciers in Alaska (DEM resolutions of

498 5 m) where elevation and Sx were the only significant parameters for all glaciers; Sx regression coefficients

499 were smaller than elevation regression coefficients, and in some cases, negative. While our results point to

500 wind having an impact on snow distribution, ~~but~~ the wind redistribution parameter (Sx) may not adequately

501 capture these effects at our study sites. For example, Glacier 4 is located in a curved valley with steep side

502 walls, so specifying a single cardinal direction for wind may not be adequate. Further, the scale of deposition

503 may be smaller than the resolution of the Sx parameter estimated from the DEM. ~~Our results corroborate~~

504 ~~those of McGrath and others (2015) in a study of six glaciers in Alaska (DEM resolutions of 5 m) where~~

505 ~~elevation and Sx were the only significant parameters for all glaciers; Sx regression coefficients were smaller~~

506 ~~than elevation regression coefficients, and in some cases, negative. In addition to wind redistribution,~~ Creation

507 of a parametrization for sublimation from blowing snow ~~has also~~, which has been shown to be an important

508 mechanism of mass loss from ridges (e.g. Musselman and others, 2015)~~. Incorporating such losses, as well~~

509 ~~as redistribution and preferential deposition, may be important for improving representations of distributed~~

510 ~~winter balance~~, may also improve explanatory power of LR for our study sites.

511 We find that transfer of LR coefficients between glaciers results in large estimation errors. Regression

512 coefficients from Glacier 4 produce the highest ~~root mean squared error~~ RMSE (0.38 m w.e. on Glacier 2 and

513 0.40 m w.e. on Glacier 13, see Table 4 for comparison) and ~~glacier-wide WB~~ B_w values are the same for all

514 glaciers (0.64 m w.e.) due to the dominance of the regression intercept. Even if the ~~regression~~ LR is performed

with ~~WB~~ b_w values from all glaciers combined, the resulting coefficients produce large ~~root mean squared errors~~ RMSE when applied to individual glaciers (0.31 m w.e., 0.15 m w.e. and 0.14 m w.e. for Glaciers 4, 2 and 13, respectively). Our results are consistent with those of Grünewald and others (2013), who found that local statistical models cannot be transferred across basins and that regional-scale models are not able to explain the majority of observed variance in winter balance.

~~Simple~~ Ordinary kriging

~~Fitted kriging parameters, including the nugget and spatial correlation length, can provide insight into important scales of winter-balance variability. The model fitted to the gridcell-averaged values of WB for Glacier 4 has a short correlation length (90 m) and large nugget (see Supplementary Material Table S3), suggesting variability in winter balance at smaller scales. Conversely, Glaciers 2 and 13 have longer correlation lengths (~450 m) and smaller nuggets, suggesting variability at larger scales. Additionally, simple kriging is better able to estimate values of WB for Glaciers 2 and 13 than for Glacier 4 (Fig. 6).~~ Due to a paucity of data, simple kriging produces almost uniform gridcell-estimated ~~values of winter balance~~ b_w in the accumulation area of each glacier, inconsistent with observations described in the literature (e.g. Machguth and others, 2006; Grabiec and others, 2011). ~~Extrapolation using simple kriging~~ Glacier 4 has the highest estimated mean with large deviations from the mean at measurement locations. The longer correlation lengths of the data for Glaciers 2 and 13 result in a more smoothly varying distributed b_w. As expected, extrapolation using OK leads to large uncertainty (Fig. 5), further emphasizing the need for spatially distributed point-scale measurements.

LR and ~~SK~~ OK comparison

~~Glacier-wide WB estimates found using both LR and SK are~~ LR and OK produce similar estimates of distributed b_w (Fig. 5) and B_w (~~0.58~~~0.60 m w.e., Table 4) for Glacier 4 but both are relatively poor predictors of ~~WB~~ b_w in measured gridcells (~~Table 4~~Fig. 6). For Glaciers 2 and 13, ~~SK~~ OK estimates are more than ~~0.1~~~0.22 m w.e. (~~up to 40%)~~39%) and ~0.11 m w.e. (30%) lower than LR estimates, respectively (Table 4). RMSE as a percentage of the ~~glacier-wide WB are comparable between LR and SK (Table 4) with an average RMSE of 22%. This comparability is interesting, given that all of the data were used to generate the SK model, while only 2/3 were used in the LR~~B_w is lower for OK than LR only for Glacier 4 but the absolute RMSE of OK is ~0.03 m w.e. lower for all glaciers, likely because OK is a data-fitting interpolation method (Table 4). Gridcell-estimated values of ~~WB~~ b_w found using LR and ~~SK~~ OK differ markedly in the upper accumulation areas of Glaciers 2 and 13~~(Fig. ??)~~, where observations are sparse and topographic parameters,

such as elevation, vary considerably. The influence of elevation results in substantially higher LR-estimated values of ~~WB~~ $b_{\rm w}$ at high elevation, whereas ~~SK-estimated values approximate the nearest data~~OK-estimated values are more uniform. Estimates of ablation-area-wide ~~WB~~ $B_{\rm w}$ differ by <~~7~~6% between LR and ~~SK~~ OK on each glacier, further emphasizing the combined ~~role~~ influence of interpolation method and measurement scarcity in the accumulation area on ~~glacier-wide WB~~ $B_{\rm w}$ estimates.

~~Distributions of glacier-wide winter balance (WB) for Glaciers 4 (G4), 2 (G2) and 13 (G13) that arise from various sources of uncertainty. WB distribution arising from grid-scale uncertainty ($\sigma_{\rm GS}$) (left column). WB distribution arising from interpolation uncertainty (σ_{INT}) (middle column). WB distribution arising from a combination of $\sigma_{\rm GS}$, $\sigma_{\rm INT}$ and density assignment uncertainty (σ_ρ) (right column). Results are shown for interpolation by linear regression (LR, top row) and simple kriging (SK, bottom row). Left two columns include eight distributions per glacier (colour) and each corresponds to a density assignment method (S1–S4 and F1–F4).~~

Uncertainty analysis using a Monte Carlo approach

~~Uncertainty analysis~~

~~Glacier-wide winter balance is affected by uncertainty introduced by the representativeness of gridcell-averaged values of WB ($\sigma_{\rm GS}$), choosing a method of density assignment (σ_ρ), and interpolating WB values across the domain ($\sigma_{\rm INT}$). Using a Monte Carlo analysis, we find that interpolation uncertainty contributes more to WB uncertainty than grid-scale uncertainty or density assignment method. In other words, the distribution of glacier-wide WB that arises from grid-scale uncertainty and the differences in distributions between methods of density assignment are smaller than the distribution that arises from interpolation uncertainty (Fig. 7 and Table 5). The WB distributions obtained using LR and SK overlap for a given glacier, but the distribution modes differ (Fig. 7). For reasons outlined above, SK-estimated values of WB in the accumulation area are generally lower, which lowers the glacier-wide WB estimate. The uncertainty in SK-estimated values of WB is large, and unrealistic glacier-wide values of WB of 0 m w.e. can be estimated (Fig. 7). Our~~ Interpolation/extrapolation of $b_{\rm w}$ data is the largest contributor of $B_{\rm w}$ uncertainty in our study. These results caution strongly against including ~~extrapolated values of WB~~ values of $B_{\rm w}$ in comparisons with remote sensing- or model-derived estimates of ~~WB~~$B_{\rm w}$. If possible, such comparisons should be restricted to point-scale data.

~~Standard deviation ($\times 10^{-2}$ m w.e.) of glacier-wide winter balance distributions arising from uncertainties in grid-scale WB ($\sigma_{\rm GS}$), density assignment (σ_ρ), interpolation ($\sigma_{\rm INT}$) and all three sources combined ($\sigma_{\rm ALL}$)~~

575 ~~for linear regression (left columns) and simple kriging (right columns)~~ σ_{GS} σ_ρ σ_{INT} σ_{ALL} σ_{GS} σ_ρ σ_{INT} σ_{ALL}

576 **Glacier 4** ~~0.86 1.90 2.13 2.90 0.85 2.15 14.05 14.72~~ **Glacier 2** ~~1.80 3.37 3.09 4.90 2.53 2.03 13.78 13.44~~

577 **Glacier 13** ~~1.12 1.68 2.80 3.20 1.15 1.27 9.65 10.43~~

578 Grid-scale uncertainty (σ_{GS}) is the smallest assessed contributor to overall ~~WB~~ B_w uncertainty. This result

579 is consistent with the generally smoothly-varying snow depths encountered in zigzag surveys, and previously

580 reported ice-roughness lengths on the order of centimetres (e.g. Hock, 2005) compared to snow depths on the

581 order of decimetres to metres. Given our assumption that zigzags are an adequate representation of grid-scale

582 variability, the low ~~WB~~ B_w uncertainty arising from σ_{GS} implies that subgrid-scale sampling need not be a

583 high priority for reducing overall uncertainty. Our assumption that the 3–4 zigzag surveys can be used to

584 estimate glacier-wide σ_{GS} may be flawed, particularly in areas with debris cover, crevasses and steep slopes.

585 Our analysis did not include uncertainty arising from ~~a number of sources, which we assume either to~~

586 ~~be encompassed by the sources investigated or to be negligible contributors. These sources of uncertainty~~

587 ~~include~~ density measurement errors associated with the ~~Federal Sampler~~FS, wedge cutters and spring scales,

588 from vertical and horizontal errors in the DEM ~~and~~ or from error associated with estimating measurement

589 locations ~~.~~

590 ~~The values of glacier-wide WB for our study glaciers (using LR and S2 density assignment method), with~~

591 ~~an uncertainty equal to one standard deviation of the distribution found with Monte Carlo analysis, are:~~

592 ~~0.59 ± 0.03 m w. e. for Glacier 4, 0.61 ± 0.05 m w.e. for Glacier 2 and 0.40 ± 0.03 m w.e. for Glacier 13. The~~

593 ~~glacier-wide WB uncertainty from combined~~ based on the GPS position of the lead observer. We assume that

594 these sources of uncertainty ~~ranges from 0.03 m w. e (5%) to 0.05 m w.e (8%) for linear-regression estimates~~

595 ~~and from 0.10 m w.e (37%) to 0.15 m w.e (24%) for simple-kriging estimates (Table 4).~~ are either encompassed

596 by the sources investigated or are negligible.

597 ~~Context and caveats~~Regional winter-balance gradient

598 *Regional winter-balance gradient*

599 Although we find considerable inter- and intra-basin variability in winter balance, our results are consistent

600 with a regional-scale winter-balance gradient for the continental side of the St. Elias Mountains (Fig. 9).

601 Winter-balance data are compiled from Taylor-Barge (1969), the three glaciers presented in this paper and

602 two ~~snow pits~~ SP we analyzed near the head of the Kaskawulsh Glacier between 20–21 May 2016. The

603 data show a linear decrease of 0.024 m w.e. km^{-1} ($R^2 = 0.85$) in winter balance with distance from the

604 regional topographic divide between the Kaskawulsh and Hubbard Glaciers, as identified by Taylor-Barge
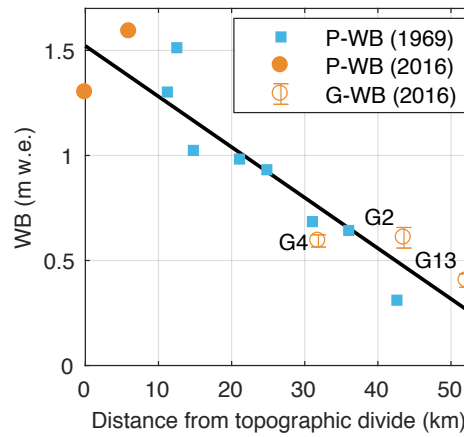
Fig. 9. Relationship between winter balance ~~(WB)~~ and linear distance from the regional topographic divide between the Kaskawulsh and Hubbard Glaciers in the St. Elias Mountains. Point-scale values of ~~WB~~ <u>winter balance</u> from snow-pit data reported by Taylor-Barge (1969) (blue boxes, P-WB). LR-estimated glacier-wide ~~WB~~ <u>winter balance</u> (B_w) calculated using density assignment S2 for Glaciers 4 (G4), 2 (G2) and 13 (G13) with errors bars calculated as the standard deviation of Monte Carlo-derived ~~WB~~ B_w distributions (this study) (open orange circles, G-WB). Point-scale ~~WB~~ <u>winter balance</u> estimated from snow-pit data at two locations in the accumulation area of the Kaskawulsh Glacier, collected in May 2016 (unpublished data, SFU Glaciology Group) (filled orange dots, P-WB). Black line indicates best fit ($R^2 = 0.85$).

(1969). While the three study glaciers fit the regional trend, the same relationship would not apply if just the Donjek Range were considered. We hypothesize that interaction between meso-scale weather patterns and large-scale mountain topography is a major driver of regional-scale winter balance. Further insight into regional-scale patterns of winter balance in the St. Elias Mountains could be gained by investigating moisture source trajectories and the contribution of orographic precipitation.

~~*Limitations and future work*~~

<u>Limitations and future work</u>

The potential limitations of our work include the restriction of our data to a single year, minimal sampling in the accumulation area, the problem of uncorrelated SP- and FS-derived densities, a sampling design that could not be optimized ~~a priori~~ *a priori*, the assumption of spatially uniform subgrid variability and lack of more finely resolved DEMs.

Inter-annual variability in winter balance is not considered in our study. A number of studies have found temporal stability in spatial patterns of snow distribution and that statistical models based on topographic parameters could be applied reliably between years (e.g. Grünewald and others, 2013). For example, Walmsley

(2015) analyzed more than 40 years of winter balance recorded on two Norwegian glaciers and found that snow distribution is spatially heterogeneous yet exhibits robust temporal stability. Contrary to this, Crochet and others (2007) found that snow distribution in Iceland differed considerably between years and depended primarily on the dominant wind direction over the course of a winter. Therefore, multiple years of snow depth and density measurements, that are not necessarily consecutive, are needed to better understand inter-annual variability ~~in winter-balance distribution~~ of winter balance within the Donjek Range.

There is a conspicuous lack of data in the accumulation areas of our study glaciers. With increased sampling in the accumulation area, interpolation uncertainties would be reduced where they are currently greatest and the ~~linear regression~~ LR would be better constrained. Although certain regions of the glaciers remain inaccessible for direct measurements, other methods of obtaining winter-balance measurements, including ground-penetrating radar and DEM differencing with photogrammetry or lidar, could be used in conjunction with manual probing to increase the spatial coverage of measurements.

The lack of correlation between SP- and FS-derived densities needs to be reconciled. Contrary to our results, most studies that compare SP- and FS-derived densities report minimal discrepancy (e.g. Dixon and Boon, 2012, and sources within). Additional co-located density measurements are needed to better compare the two methods of obtaining density values. Comparison with other ~~Federal Samplers~~ FS would also be informative. Even with this limitation, density assignment was, fortunately, not the largest source of uncertainty in estimating glacier-wide winter balance.

Our sampling design was chosen to achieve broad spatial coverage of the ablation area, but is likely too finely resolved along transects for many mass-balance surveys to replicate. An optimal sampling design would minimize uncertainty in winter balance while reducing the number of required measurements. Analysis of the estimated winter balance obtained using subsets of the data is underway to make recommendations on optimal transect configuration and along-track spacing of measurements. López-Moreno and others (2010) found that 200–400 observations are needed within a non-glacierized alpine basin ($6\,\mathrm{km}^2$) to obtain accurate and robust snow distribution models. Similar guidelines would be useful for glacierized environments.

In this study, we assume that the subgrid variability of winter balance is uniform across a given glacier. Contrary to this assumption, McGrath and others (2015) found greater variability of winter-balance values close to the terminus. Testing our assumption could be a simple matter of prioritizing the labour-intensive zigzags surveys. To ensure consistent quantification of subgrid variability, zigzag survey measurements could also be tested against other measurements methods, such as lidar.

649   DEM gridcell size is known to influence values of computed topographic parameters (Zhang and

650   Montgomery, 1994; Garbrecht and Martz, 1994; Guo-an and others, 2001; López-Moreno and others, 2010).

651   The relationship between topographic parameters and winter balance is, therefore, not independent of DEM

652   gridcell size. For example, Kienzle (2004) and López-Moreno and others (2010) found that a decrease in spatial

653   resolution of the DEM results in a decrease in the importance of curvature and an increase in the importance

654   of elevation in ~~regressions~~ LR of snow distribution on topographic parameters in non-glacierized basins. The

655   importance of curvature in our study is affected by the DEM smoothing that we applied to obtain a spatially

656   continuous curvature field (see Supplementary Material, Fig. S1). A comparison of regression coefficients

657   from high-resolution DEMs obtained from various sources and sampled with various gridcell sizes could be

658   used to characterize the dependence of topographic parameters on DEMs, and therefore assess the robustness

659   of inferred relationships between winter balance and topographic parameters.

660   **CONCLUSION**

661   We estimate winter balance for three glaciers (termed Glacier 2, Glacier 4 and Glacier 13) in the St. Elias

662   Mountains, Yukon, Canada from multiscale snow depth and density measurements. Linear regression and

663   ~~simple~~ ordinary kriging are used to obtain estimates of distributed winter balance (b_{w}). We use Monte

664   Carlo analysis to evaluate the contributions of interpolation, ~~the~~ assignment of snow density and grid-scale

665   variability of winter balance to uncertainty in estimates of glacier-wide winter balance (B_{w}).

666   Values of ~~glacier-wide winter balance~~ B_{w} estimated using linear regression and ~~simple~~ ordinary kriging

667   differ by up to $0.24\,\mathrm{m\,w.e.}$ ($\sim$50%). We find that interpolation uncertainty is the largest assessed source of

668   uncertainty in ~~glacier-wide winter balance (5~~ B_{w} (7% for linear-regression estimates and ~~32% for simple-kriging~~

669   34% for ordinary-kriging estimates). Uncertainty resulting from the method of density assignment is

670   comparatively low, despite the wide range of methods explored. Given our representation of grid-scale

671   variability, the resulting ~~winter balance~~ B_{w} uncertainty is small indicating that extensive subgrid-scale

672   sampling is not required to reduce overall uncertainty.

673   Our results suggest that processes governing distributed ~~winter balance~~ b_{w} differ between glaciers,

674   highlighting the importance of regional-scale winter-balance studies. The estimated distribution of ~~winter~~

675   ~~balance~~ b_{w} on Glacier 4 is characterized by high variability, as indicated by the poor correlation between

676   estimated and observed values and large number of data outliers. Glaciers 2 and 13 appear to have lower

677   spatial variability, with elevation being the dominant predictor of gridcell-averaged ~~winter balance~~ b_{w}. A

678   wind-redistribution parameter is found to be a weak but significant predictor of ~~winter balance~~ b_{w}, though

conflicting relationships between glaciers make it difficult to interpret. The major limitations of our work include the restriction of our data to a single year and minimal sampling in the accumulation area. Although challenges persist when estimating winter balance, our data are consistent with a regional-scale winter-balance gradient for the continental side of the St. Elias Mountains.

AUTHOR CONTRIBUTION STATEMENT

AP planned and executed the data collection, performed all calculations and drafted the manuscript. GF conceived of the study, contributed to field planning and data collection, oversaw all stages of the work and edited the manuscript. VR provided guidance with statistical methods and edited the manuscript.

ACKNOWLEDGEMENTS

REFERENCES

Anderton S, White S and Alvera B (2004) Evaluation of spatial variability in snow water equivalent for a high mountain catchment. *Hydrological Processes*, **18**(3), 435–453 (doi: 10.1002/hyp.1319)

Arendt AA, Luthcke SB, Larsen CF, Abdalati W, Krabill WB and Beedle MJ (2008) Validation of high-resolution GRACE mascon estimates of glacier mass changes in the St Elias Mountains, Alaska, USA, using aircraft laser altimetry. *Journal of Glaciology*, **54**(188), 778–787 (doi: 10.3189/002214308787780067)

Bagos PG and Adam M (2015) On the Covariance of Regression Coefficients. *Open Journal of Statistics*, **5**, 680–701 (doi: 10.4236/ojs.2015.57069)

706 Balk B and Elder K (2000) Combining binary decision tree and geostatistical methods to estimate snow distribution

707   in a mountain watershed. *Water Resources Research*, **36**(1), 13–26 (doi: 10.1029/1999WR900251)

708 Barry RG (1992) *Mountain weather and climate*. Cambridge Univserity Press, 3rd edition

709 Beaumont RT and Work RA (1963) Snow sampling results from three samplers. *International Association of Scientific*

710   *Hydrology. Bulletin*, **8**(4), 74–78 (doi: 10.1080/02626666309493359)

711 Braithwaite RJ (2008) Temperature and precipitation climate at the equilibrium-line altitude of glaciers expressed by

712   the degree-day factor for melting snow. *Journal of Glaciology*, **54**(186), 437–444 (doi: 10.3189/002214308785836968)

713 Burgess EW, Forster RR and Larsen CF (2013) Flow velocities of Alaskan glaciers. *Nature communications*, **4**,

714   2146–2154 (doi: 10.1038/ncomms3146)

715 Burnham KP and Anderson DR (2004) Multimodel Inference: Understanding AIC and BIC in Model Selection.

716   *Sociological Methods & Research*, **33**(2), 261–304 (doi: 10.1177/0049124104268644)

717 Carroll T (1977) A comparison of the CRREL 500 cm^3 tube and the ILTS 200 and 100 cm^3 box cutters used for

718   determining snow densities. *Journal of Glaciology*, **18**(79), 334–337 (doi: 10.1017/S0022143000021420)

719 Clark MP, Hendrikx J, Slater AG, Kavetski D, Anderson B, Cullen NJ, Kerr T, Örn Hreinsson E and Woods RA

720   (2011) Representing spatial variability of snow water equivalent in hydrologic and land-surface models: A review.

721   *Water Resources Research*, **47**(7) (doi: 10.1029/2011WR010745)

722 Clarke GK (2014) A short and somewhat personal history of Yukon glacier studies in the Twentieth Century. *Arctic*,

723   **37**(1), 1–21

724 Clyde GD (1932) Circular No. 99-Utah Snow Sampler and Scales for Measuring Water Content of Snow. *UAES*

725   *Circulars*, Paper 90

726 Cogley J, Hock R, Rasmussen L, Arendt A, Bauder A, Braithwaite R, Jansson P, Kaser G, Möller M, Nicholson L

727   and others (2011) *Glossary of glacier mass balance and related terms*. UNESCO-IHP, Paris

728 Conger SM and McClung DM (2009) Comparison of density cutters for snow profile observations. *Journal of*

729   *Glaciology*, **55**(189), 163–169 (doi: 10.3189/002214309788609038)

730 Crochet P, Jóhannesson T, Jónsson T, SigurÃřsson O, Björnsson H, Pálsson F and Barstad I (2007) Estimating

731   the Spatial Distribution of Precipitation in Iceland Using a Linear Model of Orographic Precipitation. *Journal of*

732   *Hydrometeorology*, **8**(6), 1285–1306 (doi: 10.1175/2007JHM795.1)

733 Crompton JW and Flowers GE (2016) Correlations of suspended sediment size with bedrock lithology and glacier

734   dynamics. *Annals of Glaciology*, **57**(72), 1–9 (doi: 10.1017/aog.2016.6)

735 Cullen NJ, Anderson B, Sirguey P, Stumm D, Mackintosh A, Conway JP, Horgan HJ, Dadic R, Fitzsimons SJ

736   and Lorrey A (2017) An 11-year record of mass balance of Brewster Glacier, New Zealand, determined using a

737   geostatistical approach. *Journal of Glaciology*, **63**(238), 199–217 (doi: 10.1017/jog.2016.128)

738 Dadić R, Mott R, Lehning M and Burlando P (2010) Parameterization for wind-induced preferential deposition of
739   snow. *Journal of Geophysical Research: Earth Surface*, **24**(14), 1994–2006 (doi: 10.1029/2009JF001261)

740 Danby RK, Hik DS, Slocombe DS and Williams A (2003) Science and the St. Elias: an evolving framework
741   for sustainability in North America's highest mountains. *The Geographical Journal*, **169**(3), 191–204 (doi:
742   10.1111/1475-4959.00084)

743 Davis JC and Sampson RJ (1986) *Statistics and data analysis in geology*. Wiley New York et al., 2nd edition

744 Deems JS and Painter TH (2006) Lidar measurement of snow depth: accuracy and error sources. In *Proceedings of
745   the International Snow Science Workshop*

746 Dixon D and Boon S (2012) Comparison of the SnowHydro snow sampler with existing snow tube designs. *Hydrological
747   Processes*, **26**(17), 2555–2562 (doi: 10.1002/hyp.9317)

748 Egli L, Griessinger N and Jonas T (2011) Seasonal development of spatial snow-depth variability across different
749   scales in the Swiss Alps. *Annals of Glaciology*, **52**(58), 216–222 (doi: 10.3189/172756411797252211)

750 Elder K, Dozier J and Michaelsen J (1991) Snow accumulation and distribution in an alpine watershed. *Water
751   Resources Research*, **27**(7), 1541–1552 (doi: 10.1029/91WR00506)

752 Elder K, Rosenthal W and Davis RE (1998) Estimating the spatial distribution of snow water equiv-
753   alence in a montane watershed. *Hydrological Processes*, **12**(1011), 1793–1808 (doi: 10.1002/(SICI)1099-
754   1085(199808/09)12:10/111793::AID-HYP6953.0.CO;2-K)

755 Erxleben J, Elder K and Davis R (2002) Comparison of spatial interpolation methods for estimating snow distribution
756   in the Colorado Rocky Mountains. *Hydrological Processes*, **16**(18), 3627–3649 (doi: 10.1002/hyp.1239)

757 Fames PE, Peterson N, Goodison B and Richards RP (1982) Metrication of Manual Snow Sampling Equipment. In
758   *Proceedings of the 50th Western Snow Conference*, 120–132

759 Fierz C, Armstrong RL, Durand Y, Etchevers P, Greene E, McClung DM, Nishimura K, Satyawali PK and Sokratov
760   SA (2009) *The international classification for seasonal snow on the ground*. UNESCO/IHP, unesco/ihp paris
761   edition

762 Garbrecht J and Martz L (1994) Grid size dependency of parameters extracted from digital elevation models.
763   *Computers & Geosciences*, **20**(1), 85–87 (doi: 10.1016/0098-3004(94)90098-1)

764 Gerber F, Lehning M, Hoch SW and Mott R (2017) A close-ridge small-scale atmospheric flow field and its
765   influence on snow accumulation. *Journal of Geophysical Research: Atmospheres*, **122**(15), 7737–7754 (doi:
766   10.1002/2016JD026258), 2016JD026258

767 Grabiec M, Puczko D, Budzik T and Gajek G (2011) Snow distribution patterns on Svalbard glaciers derived from
768   radio-echo soundings. *Polish Polar Research*, **32**(4), 393–421 (doi: 10.2478/v10183-011-0026-4)

769 Gray DM and Male DH (1981) *Handbook of snow: principles, processes, management & use*. Pergamon Press, 1st
770   edition

771 Grünewald T, Schirmer M, Mott R and Lehning M (2010) Spatial and temporal variability of snow depth and ablation
772   rates in a small mountain catchment. *Cryosphere*, **4**(2), 215–225 (doi: 10.5194/tc-4-215-2010)

773 Grünewald T, Stötter J, Pomeroy J, Dadic R, Moreno Baños I, Marturià J, Spross M, Hopkinson C, Burlando P
774   and Lehning M (2013) Statistical modelling of the snow depth distribution in open alpine terrain. *Hydrology and
775   Earth System Sciences*, **17**(8), 3005–3021 (doi: 10.5194/hess-17-3005-2013)

776 Grünewald T, Bühler Y and Lehning M (2014) Elevation dependency of mountain snow depth. *The Cryosphere*, **8**(6),
777   2381–2394 (doi: 10.5194/tc-8-2381-2014)

778 Guo-an T, Yang-he H, Strobl J and Wang-qing L (2001) The impact of resolution on the accuracy of hydrologic data
779   derived from DEMs. *Journal of Geographical Sciences*, **11**(4), 393–401 (doi: 10.1007/BF02837966)

780 Gusmeroli A, Wolken GJ and Arendt AA (2014) Helicopter-borne radar imaging of snow cover on and around glaciers
781   in Alaska. *Annals of Glaciology*, **55**(67), 78–88 (doi: 10.3189/2014AoG67A029)

782 Hagen JO and Liestøl O (1990) Long-term glacier mass-balance investigations in Svalbard, 1950-88. *Annals of
783   Glaciology*, **14**(1), 102–106

784 Helbig N and van Herwijnen A (2017) Subgrid parameterization for snow depth over mountainous terrain from flat
785   field snow depth. *Water Resources Research*, **53**(2), 1444–1456 (doi: 10.1002/2016WR019872)

786 Hock R (2005) Glacier melt: a review of processes and their modelling. *Progress in Physical Geography*, **29**(3), 362–391
787   (doi: 10.1191/0309133305pp453ra)

788 Hock R and Jensen H (1999) Application of kriging interpolation for glacier mass balance computations. *Geografiska
789   Annaler: Series A, Physical Geography*, **81**(4), 611–619 (doi: 10.1111/1468-0459.00089)

790 Kaser G, Fountain A, Jansson P and others (2003) *A manual for monitoring the mass balance of mountain glaciers.*
791   ICSI/UNESCO

792 Kienzle S (2004) The Effect of DEM Raster Resolution on First Order, Second Order and Compound Terrain
793   Derivatives. *Transactions in GIS*, **8**(1), 83–111 (doi: 10.1111/j.1467-9671.2004.00169.x)

794 Kinar N and Pomeroy J (2015) Measurement of the physical properties of the snowpack. *Reviews of Geophysics*,
795   **53**(2), 481–544 (doi: 10.1002/2015RG000481)

796 Kohavi R and others (1995) A study of cross-validation and bootstrap for accuracy estimation and model selection.
797   In *Proceedings of the Fourteenth International Joint Conference on Artificial Intelligence*, 1137–1145

798 Korona J, Berthier E, Bernard M, Rémy F and Thouvenot E (2009) SPIRIT SPOT 5 stereoscopic survey of Polar
799   Ice: Reference images and topographies during the fourth International Polar Year (2007–2009). *ISPRS Journal
800   of Photogrammetry and Remote Sensing*, **64**(2), 204–212 (doi: 10.1016/j.isprsjprs.2008.10.005)

801 Lehning M, Völksch I, Gustafsson D, Nguyen TA, Stähli M and Zappa M (2006) ALPINE3D: a detailed model of
802   mountain surface processes and its application to snow hydrology. *Hydrological Processes*, **20**(10), 2111–2128 (doi:
803   10.1002/hyp.6204)

804 Li J and Heap AD (2008) A review of spatial interpolation methods for environmental scientists. *Geoscience Australia,*
805   Record 2008/23

806 Liston GE and Elder K (2006) A distributed snow-evolution modeling system (SnowModel). *Journal of*
807   *Hydrometeorology*, **7**(6), 1259–1276 (doi: 10.1175/JHM548.1)

808 Liston GE and Sturm M (1998) A snow-transport model for complex terrain. *Journal of Glaciology*, **44**(148), 498–516

809 López-Moreno J, Latron J and Lehmann A (2010) Effects of sample and grid size on the accuracy and stability of
810   regression-based snow interpolation methods. *Hydrological Processes*, **24**(14), 1914–1928 (doi: 10.1002/hyp.7564)

811 López-Moreno J, Fassnacht S, Heath J, Musselman K, Revuelto J, Latron J, Morán-Tejeda E and Jonas T (2013)
812   Small scale spatial variability of snow density and depth over complex alpine terrain: Implications for estimating
813   snow water equivalent. *Advances in Water Resources*, **55**, 40–52 (doi: 10.1016/j.advwatres.2012.08.010)

814 López-Moreno JI, Fassnacht S, Beguería S and Latron J (2011) Variability of snow depth at the plot scale: implications
815   for mean depth estimation and sampling strategies. *The Cryosphere*, **5**(3), 617–629 (doi: 10.5194/tc-5-617-2011)

816 MacDougall AH and Flowers GE (2011) Spatial and temporal transferability of a distributed energy-balance glacier
817   melt model. *Journal of Climate*, **24**(5), 1480–1498 (doi: 10.1175/2010JCLI3821.1)

818 Machguth H, Eisen O, Paul F and Hoelzle M (2006) Strong spatial variability of snow accumulation observed
819   with helicopter-borne GPR on two adjacent alpine glaciers. *Geophysical Research Letters*, **33**(13), 1–5 (doi:
820   10.1029/2006GL026576)

821 Madigan D and Raftery AE (1994) Model Selection and Accounting for Model Uncertainty in Graphical Models
822   Using Occam's Window. *Journal of the American Statistical Association*, **89**(428), 1535–1546

823 Marshall HP, Koh G, Sturm M, Johnson J, Demuth M, Landry C, Deems J and Gleason J (2006) Spatial variability of
824   the snowpack: Experiences with measurements at a wide range of length scales with several different high precision
825   instruments. In *Proceedings International Snow Science Workshop*, 359–364

826 McGrath D, Sass L, O'Neel S, Arendt A, Wolken G, Gusmeroli A, Kienholz C and McNeil C (2015) End-of-winter
827   snow depth variability on glaciers in Alaska. *Journal of Geophysical Research: Earth Surface*, **120**(8), 1530–1550
828   (doi: 10.1002/2015JF003539)

829 Metropolis N and Ulam S (1949) The Monte Carlo Method. *Journal of the American Statistical Association*, **44**(247),
830   335–341

831 Molotch N, Colee M, Bales R and Dozier J (2005) Estimating the spatial distribution of snow water equivalent in
832   an alpine basin using binary regression tree models: the impact of digital elevation data and independent variable
833   selection. *Hydrological Processes*, **19**(7), 1459–1479 (doi: 10.1002/hyp.5586)

834 Mott R, Faure F, Lehning M, Löwe H, Hynek B, Michlmayer G, Prokop A and Schöner W (2008) Simulation of
835   seasonal snow-cover distribution for glacierized sites on Sonnblick, Austria, with the Alpine3D model. *Annals of*
836   *Glaciology*, **49**(1), 155–160 (doi: 10.3189/172756408787814924)

Musselman KN, Pomeroy JW, Essery RL and Leroux N (2015) Impact of windflow calculations on simulations of alpine snow accumulation, redistribution and ablation. *Hydrological Processes*, **29**(18), 3983–3999 (doi: 10.1002/hyp.10595)

Proksch M, Rutter N, Fierz C and Schneebeli M (2016) Intercomparison of snow density measurements: bias, precision, and vertical resolution. *The Cryosphere*, **10**(1), 371–384 (doi: 10.5194/tc-10-371-2016)

Pulwicki A (2017) *Multi-scale investigation of winter balance on alpine glaciers.* Master's thesis, Simon Fraser University

Raftery AE, Madigan D and Hoeting JA (1997) Bayesian Model Averaging for Linear Regression Models. *Journal of the American Statistical Association*, **92**(437), 179–191 (doi: 10.1080/01621459.1997.10473615)

Rasmussen CE and Williams CK (2006) *Gaussian processes for machine learning.* MIT press Cambridge

Réveillet M, Vincent C, Six D and Rabatel A (2016) Which empirical model is best suited to simulate glacier mass balances? *Journal of Glaciology*, **63**(237), 1–16 (doi: 10.1017/jog.2016.110)

Roustant O, Ginsbourger D and Deville Y (2012) DiceKriging, DiceOptim: Two R packages for the analysis of computer experiments by kriging-based metamodeling and optimization. *Journal of Statistical Software*, **21**, 1–55

Schneiderbauer S and Prokop A (2011) The atmospheric snow-transport model: SnowDrift3D. *Journal of Glaciology*, **57**(203), 526–542 (doi: 10.3189/002214311796905677)

Schuler TV, Crochet P, Hock R, Jackson M, Barstad I and Jóhannesson T (2008) Distribution of snow accumulation on the Svartisen ice cap, Norway, assessed by a model of orographic precipitation. *Hydrological Processes*, **22**(19), 3998–4008 (doi: 10.1002/hyp.7073)

Scipión DE, Mott R, Lehning M, Schneebeli M and Berne A (2013) Seasonal small-scale spatial variability in alpine snowfall and snow accumulation. *Water Resources Research*, **49**(3), 1446–1457, ISSN 1944-7973 (doi: 10.1002/wrcr.20135)

Shea C and Jamieson B (2010) Star: an efficient snow point-sampling method. *Annals of Glaciology*, **51**(54), 64–72 (doi: 10.3189/172756410791386463)

Sold L, Huss M, Hoelzle M, Andereggen H, Joerg PC and Zemp M (2013) Methodological approaches to infer end-of-winter snow distribution on alpine glaciers. *Journal of Glaciology*, **59**(218), 1047–1059 (doi: 10.3189/2013JoG13J015)

Tangborn WV, Krimmel RM and Meier MF (1975) A comparison of glacier mass balance by glaciological, hydrological and mapping methods, South Cascade Glacier, Washington. *International Association of Hydrological Sciences Publication*, **104**, 185–196

Taylor-Barge B (1969) *The summer climate of the St. Elias Mountain region.* Montreal: Arctic Institute of North America, Research Paper No. 53

869 Thibert E, Blanc R, Vincent C and Eckert N (2008) Glaciological and volumetric mass-balance measurements: error

870   analysis over 51 years for Glacier de Sarennes, French Alps. *Journal of Glaciology*, **54**(186), 522–532

871 Trujillo E and Lehning M (2015) Theoretical analysis of errors when estimating snow distribution through point

872   measurements. *The Cryosphere*, **9**(3), 1249–1264 (doi: 10.5194/tc-9-1249-2015)

873 Turcan J and Loijens H (1975) Accuracy of snow survey data and errors in snow sampler measurements. In *32nd*

874   *Eastern Snow Conference*

875 Tveit J and Killingtveit Å (1994) Snow surveys for studies of water budget on Svalbard 1991–1994. In *Proceedings*

876   *of the 10th International Northern Research Basins Symposium and Workshop, Spitsbergen, Norway. SINTEF*

877   *Report*, volume 22, A96415

878 Waechter A, Copland L and Herdes E (2015) Modern glacier velocities across the Icefield Ranges, St Elias

879   Mountains, and variability at selected glaciers from 1959 to 2012. *Journal of Glaciology*, **61**(228), 624–634 (doi:

880   10.3189/2015JoG14J147)

881 Walmsley APU (2015) *Long-term observations of snow spatial distributions at Hellstugubreen and Gråsubreen,*

882   *Norway.* Master's thesis, University of Oslo

883 Wetlaufer K, Hendrikx J and Marshall L (2016) Spatial Heterogeneity of Snow Density and Its Influence on Snow Wa-

884   ter Equivalence Estimates in a Large Mountainous Basin. *Hydrology*, **3**(3), 1–17 (doi: 10.3390/hydrology3010003)

885 Wilson N and Flowers G (2013) Environmental controls on the thermal structure of alpine glaciers. *The Cryosphere*,

886   **7**(1), 167–182 (doi: 10.5194/tc-7-167-2013)

887 Wilson NJ, Flowers GE and Mingo L (2013) Comparison of thermal structure and evolution between neighboring

888   subarctic glaciers. *Journal of Geophysical Research: Earth Surface*, **118**(3), 1443–1459 (doi: 10.1002/jgrf.20096)

889 Winstral A, Elder K and Davis RE (2002) Spatial snow modeling of wind-redistributed snow using terrain-based pa-

890   rameters. *Journal of Hydrometeorology*, **3**(5), 524–538 (doi: 10.1175/1525-7541(2002)0030524:SSMOWR2.0.CO;2)

891 Winstral A, Marks D and Gurney R (2013) Simulating wind-affected snow accumulations at catchment to basin

892   scales. *Advances in Water Resources*, **55**, 64–79 (doi: 10.1016/j.advwatres.2012.08.011)

893 Winther J, Bruland O, Sand K, Killingtveit A and Marechal D (1998) Snow accumulation distribution on Spitsbergen,

894   Svalbard, in 1997. *Polar Research*, **17**, 155–164 (doi: 10.3402/polar.v17i2.6616)

895 Woo MK and Marsh P (1978) Analysis of Error in the Determination of Snow Storage for Small High Arctic Basins.

896   *Journal of Applied Meteorology*, **17**(10), 1537–1541 (doi: 10.1175/1520-0450(1978)0171537:AOEITD2.0.CO;2)

897 Wood WA (1948) Project "Snow Cornice": the establishment of the Seward Glacial research station. *Arctic*, **1**(2),

898   107–112

899 Work R, Stockwell H, Freeman T and Beaumont R (1965) *Accuracy of field snow surveys.* Cold Regions Research &

900   Engineering Laboratory

901 Zhang W and Montgomery DR (1994) Digital elevation model grid size, landscape representation, and hydrologic

902   simulations. *Water Resources Research*, **30**(4), 1019–1028 (doi: 10.1029/93WR03553)